Atmos. Chem. Phys. Discuss., 11, 28219–28272, 2011
www.atmos-chem-phys-discuss.net/11/28219/2011/
doi:10.5194/acpd-11-28219-2011

Atmospheric Chemistry and Physics Discussions

Carbonaceous aerosols in China: top-down constraints on primary sources and estimation of secondary contribution

T.-M. Fu[1], J. J. Cao[2], X. Y. Zhang[3], S. C. Lee[4], Q. Zhang[5], Y. M. Han[2], W. J. Qu[6], Z. Han[7], R. Zhang[7], Y. X. Wang[5], D. Chen[8], and D. K. Henze[9]

[1]Department of Atmospheric and Oceanic Sciences and Laboratory for Climate and Ocean-Atmosphere Studies, School of Physics, Peking University, Beijing, China
[2]State Key Laboratory of Loess and Quaternary Geology, Institute of Earth Environment, Chinese Academy of Sciences, Xi'an, China
[3]Key Laboratory for Atmospheric Chemistry, Centre for Atmosphere Watch & Services of CMA, Chinese Academy of Meteorological Sciences, Beijing, China
[4]Research Center of Urban Environmental Technology and Management, Department of Civil and Structural Engineering, Hong Kong Polytechnic University, Kowloon, Hong Kong
[5]Ministry of Education Key Laboratory for Earth System Modeling, Center for Earth System Science, Institute for Global Change Studies, Tsinghua University, Beijing, China
[6]Physical Oceanography Laboratory, Ocean-Atmosphere Interaction and Climate Laboratory, Ocean University of China, Qingdao, China

[7]Key Laboratory of Regional Climate-Environment Research for Temperate East Asia, Institute of Atmospheric Physics, Chinese Academy of Sciences, Beijing, China
[8]Department of Atmospheric & Oceanic Sciences, University of California, Los Angeles, Los Angeles, USA
[9]Department of Mechanical Engineering, University of Colorado at Boulder, Boulder, USA

Received: 15 August 2011 – Accepted: 11 October 2011 – Published: 20 October 2011

Correspondence to: T.-M. Fu (tmfu@pku.edu.cn)

Published by Copernicus Publications on behalf of the European Geosciences Union.

Abstract

We simulate elemental carbon (EC) and organic carbon (OC) aerosols in China and compare model results to surface measurements at Chinese rural and background sites, with the goal of deriving "top-down" emission estimates of EC and OC, as well as better quantifying the secondary sources of OC. We include in the model state-of-the-science Chinese "bottom-up" emission inventories for EC ($1.92\,Tg\,C\,yr^{-1}$) and OC ($3.95\,Tg\,C\,yr^{-1}$), as well as updated secondary OC formation pathways. The average simulated annual mean EC concentration at rural and background site is $1.1\,\mu g\,C\,m^{-3}$, 56 % lower than the observed $2.5\,\mu g\,C\,m^{-3}$. The average simulated annual mean OC concentration at rural and background sites is $3.4\,\mu g\,C\,m^{-3}$, 76 % lower than the observed $14\,\mu g\,C\,m^{-3}$. Multiple regression to fit surface monthly mean EC observations at rural and background sites yields best estimate of Chinese EC source of $3.05 \pm 0.78\,Tg\,C\,yr^{-1}$. Based on the top-down EC emission estimate and observed seasonal primary OC/EC ratios, we estimate Chinese OC total emissions to be $6.67 \pm 1.30\,Tg\,C\,yr^{-1}$. Using these top-down estimates, the simulated average annual mean EC concentration at rural and background sites significantly improved to $1.9\,\mu g\,C\,m^{-3}$. However, the model still significantly underestimates observed OC in all seasons (simulated average annual mean OC at rural and background sites is $5.4\,\mu g\,C\,m^{-3}$), with little skill in capturing the spatiotemporal variability. Secondary formation accounts for 21 % of Chinese annual mean surface OC in the model, with isoprene being the most important precursor. In summer, as high as 62 % of the observed surface OC may be due to secondary formation in eastern China. Our analysis points to three shortcomings in the current bottom-up inventories of Chinese carbonaceous aerosols: (1) the anthropogenic source is severely underestimated, particularly for OC; (2) there is a missing source in western China, likely associated with the use of biofuels or other low-quality fuels for heating; and (3) sources in fall are not well represented, either because the seasonal shifting of emissions and/or secondary formation are poorly captured or because specific fall emission events are missing. More regional measurements with better spatiotemporal coverage are needed to resolve these shortcomings.

ACPD

11, 28219–28272, 2011

1 Introduction

Carbonaceous aerosols, including elemental carbon aerosol (EC) and organic carbon aerosol (OC), are important components of atmospheric particulate matter, affecting air quality and climate. EC, often referred to as black carbon aerosol (BC) depending on measurement techniques, are emitted directly into the atmosphere from combustion associated with anthropogenic activities and biomass burning. OC can be emitted as primary particles from combustion; they can also be produced in the atmosphere as part of secondary organic aerosol (SOA), formed by oxidation products of volatile organic compounds (VOC). In this study, we use surface observations to constrain the primary and secondary sources of carbonaceous aerosols in China.

Estimates of Chinese EC and OC emissions are highly uncertain (Streets et al., 2003a; Ohara et al., 2007; Zhang et al., 2009; Lei et al., 2011; Lu et al., 2011). Emission inventories are traditionally constructed "from the bottom up" base on activity data and emission factors. However, accurate and detailed activity statistics are often unavailable in China. Emission factors representative of local conditions are scarcely measured, and the values are highly variable depending on fuel type and combustion conditions, some differing by orders of magnitude from western values (Streets et al., 2001, 2003a; Bond et al., 2004; Cao et al., 2006; Ohara et al., 2007; Zhang et al., 2009; Lei et al., 2011; and references therein). As a result, there are large uncertainties associated with Chinese emissions from small industries (such as coke and brick production), residential combustion, and transportation (Zhang et al., 2009; Lu et al., 2011); all three activities are important sources of carbonaceous aerosols.

Only a few studies have examined the validity of Chinese carbonaceous aerosol emission inventories by applying them to numerical models and comparing results against observations. Hakami et al. (2005) used an adjoint model and surface measurements in and around Korea and Japan in spring 2001 to test the anthropogenic and biomass burning EC emission inventories by Streets et al. (2003a, b). They concluded that while the estimated emission totals for East Asia were consistent with observations, there were sizable sub-regional differences. In particular, anthropogenic

ACPD
11, 28219–28272, 2011

emissions from northeastern China and Japan were underestimated, while those from southeastern China were overestimated. Z. Han et al. (2008) also used the anthropogenic and biomass burning emission inventories by Streets et al. (2003a, b) to simulate summertime primary and secondary carbonaceous aerosols in eastern China. They compared model results against surface observations at 14 urban and 3 rural sites in summer 2003 and found both EC and OC to be underestimated at almost all sites. Matsui et al. (2009) calculated the anthropogenic EC and OC emissions for northern China for the year 2004, applied their inventory in a regional model, and compared simulated concentrations to observations in Beijing in summer 2006. They found that the model overestimated EC at one urban site and one suburban site in Beijing, as well as overestimated OC at the suburban site. Kondo et al. (2011) measured year-round BC concentrations on a remote island in East China Sea, downwind from China. They selectively analysed data strongly impacted by transport from China (mostly in winter and spring) and estimated Chinese annual anthropogenic BC emission to be 1.92 Tg C yr^{-1}, similar to the 1.81 Tg C yr^{-1} estimated by Zhang et al. (2009). Each of these previous studies was limited to a particular location and/or a particular season. Koch et al. (2009) analyzed results from 17 global models using different emission inventories; they found that 16 of the 17 models severely underestimated the observed annual mean surface EC concentrations in China. To the best of our knowledge, no detailed evaluation has been conducted on Chinese carbonaceous aerosol emission estimates at the national scale for all seasons.

Very little is known about the secondary sources of OC in China. Zhang et al. (2005) measured EC and OC at a coastal site in eastern China from June to December 2003 and at a sandy land site in northeastern China from June to August 2003. Based on trajectory analysis and the minimum OC/EC ratios observed in clean air masses, they found that 37–57 % of the total OC could be attributed to secondary sources. Cao et al. (2007) analyzed January and July 2003 EC and OC measurements at 14 Chinese cities and estimated that 40 % of urban surface OC is secondary. Zhang et al. (2008) analyzed year-round EC and OC measurements at 18 urban, rural, and background

ACPD
11, 28219–28272, 2011

sites. They estimated that secondary OC (SOC) accounts for 48–62 % and 53–80 % of urban and rural annual surface OC, respectively, base on the observed minimum OC/EC ratios at each site. X. Wang et al. (2009) simulated SOA in a regional chemistry model and found that 55 % to 65 % of SOA came from aromatic VOC in the Pearl River Delta region in spring. Also using a regional chemistry model, Liu et al. (2010) concluded that SOC produced from biogenic and anthropogenic VOC accounted for 20 % of annual mean surface OC in eastern China. Neither X. Wang et al. (2009) nor Liu et al. (2010) compared model results with observations. Z. Han et al. (2008) simulated summertime SOC produced by biogenic VOC in eastern China. They found that SOC made up 50 % of the simulated surface OC in the forested areas of southeastern, southwestern and northeastern China in summer, although their simulated total OC concentrations are 40 % lower than observed values. Monoterpenes, isoprene, and aromatics accounted for 48 %, 35 %, 17 % of their simulated SOC, respectively. All of the modeling studies described above considered only SOC produced by equilibrium-partitioning of semi-volatile oxidation products of VOC precursors (Pankow et al., 1994a, b; Odum et al., 1996). Recent studies indicate that additional secondary formation pathways, such as the aqueous reactions of dicarbonyls or other process not involving the aqueous phase, may be important (Herndon et al., 2008; Carlton et al., 2009; Hallquist et al., 2009).

A major obstacle in understanding the sources and distributions of Chinese carbonaceous aerosol is the lack of a consistent measurement network in China with good spatiotemporal coverage, such as the IMPROVE network in the United States (Malm et al., 1994). In the past decade, many studies measured EC and OC at Chinese urban and rural sites. However, most of such measurements were conducted at a single location for a short period of time. Only two recent published studies measured carbonaceous aerosols simultaneously at multiple locations across China in winter and summer (Cao et al., 2007) or over an entire year (Zhang et al., 2008). The spatial and seasonal variability of these measurements provide important information about the sources of carbonaceous aerosols.

ACPD
11, 28219–28272, 2011

The goal of this study is to quantify the primary and secondary sources of Chinese carbonaceous aerosols by comparing numerical simulations against observations country-wide for all seasons. A database of surface EC and OC measurements at background, rural, and urban locations is compiled from previous studies to represent the spatial and seasonal variability. We conduct a year-long simulation of carbonaceous aerosols in China, incorporating the current knowledge of primary sources and secondary formation pathways. The simulated results are then compared to seasonal surface observations at background and rural sites in China to derive "top-down" estimates for the primary EC and OC sources and to quantify the secondary formation of OC.

2 Model and data description

2.1 GEOS-Chem model

We simulate carbonaceous aerosol over East and South Asia using the one-way nested-grid capability of the GEOS-Chem 3-D chemical transport model (version 8.1.3; http://acmg.seas.harvard.edu/geos/). GEOS-Chem is driven by assimilated meteorological data from the Goddard Earth Observing System (GEOS-5) of the NASA Global Modeling Assimilation Office (Bey et al., 2001). Meteorology fields in GEOS-5 have a temporal resolution of 6 h (3 h for surface variables), a horizontal resolution of 0.667° longitude × 0.5° latitude, and 72 hybrid eta levels in the vertical direction extending from the surface to 0.01 hPa. To drive GEOS-Chem, the number of vertical levels is reduced to 47 by merging layers in the stratosphere. The lowest 2 km of the atmosphere is resolved by 14 levels. For global simulations, the horizontal resolution of meteorology fields is reduced to either 5° longitude × 4° latitude or 2.5° longitude × 2° latitude.

The one-way nested-grid capability of GEOS-Chem for East and South Asia (70° E ~ 150° E, 10° S ~ 55° N) was developed by Wang et al. (2004) and updated by Chen et al. (2009) for GEOS-5 using the native horizontal resolution (0.667°

ACPD
11, 28219–28272, 2011

longitude × 0.5° latitude). Tracer concentrations at the lateral boundaries are provided by a global GEOS-Chem simulation at 5° longitude × 4° latitude horizontal resolution and updated in the nested-grid model every 3 h. Chen et al. (2009) simulated the summertime distribution and transport of CO in China. They showed that the nested-grid model is able to resolve individual cities associated with high emission intensities, as well as reproduce the transport of urban plumes to a suburban site near Beijing. Y. Wang et al. (2009) compared results from the nested-grid model against O_3, CO, NO_y, and SO_2 measurements at a rural site downwind of Beijing. They found that the model is able to reproduce the observed pollution level changes associated with emission reductions in Beijing.

Carbonaceous aerosols in the standard GEOS-Chem model include primary EC, primary OC, as well as SOC as part of SOA produced from VOC precursor oxidation. The terms "elemental carbon aerosol" (EC) and "black carbon aerosol" (BC) are often used interchangeably in emission and modeling literature, and there are currently no universally accepted definitions for the two terms. From a measurement stand point, EC mostly refers to aerosol measured with thermal/optical techniques, while BC mostly refers to aerosol measured with photo-absorption techniques. The mass concentrations determined using these two techniques can sometimes be significantly different (Jeong et al., 2004). For the purpose of this study, we consider EC to be equivalent to BC. The "bottom-up" emission inventories of EC and OC and VOC precursors used to drive our model are described in Sect. 2.2. EC and OC are separated into hydrophilic and hydrophobic components and are removed by dry deposition (Wesley, 1989; Wang et al., 1998) and wet deposition (Liu et al., 2001; Mari et al., 2000). Freshly emitted EC and OC are assumed to be 20 % and 50 % water-soluble, respectively (Cooke et al., 1999; Park et al., 2005). The water-insoluble fraction is converted to water-soluble in the atmosphere with an e-folding lifetime of 1.15 days, constrained by observed export efficiency vertical profiles (Park et al., 2005). We conduct a sensitivity test by tripling this conversion lifetime in the nested-grid model but find the change in simulated monthly mean Chinese surface EC and OC concentrations to be less than 5 %.

ACPD
11, 28219–28272, 2011

GEOS-Chem simulates SOA formation by equilibrium partitioning of semi-volatile oxidation products from biogenic terpenes, (Liao et al., 2007), biogenic isoprene (Henze and Seinfeld, 2006), as well as aromatics from anthropogenic activities and biomass burning (Henze et al., 2008). The equilibrium partitioning is as described by Chung and Seinfeld (2002), except for this study the semi-volatile SOA is allowed to partition onto all preexisting OC and inorganic aqueous aerosols, which provides an upper estimate of semi-volatile SOA production. We assume that all semi-volatile SOA have an aerosol-to-carbon (SOA/SOC) mass ratio of 2.1 (Turpin and Lim, 2001) and are 80 % water-soluble following Chung and Seinfeld (2002).

In addition, GEOS-Chem simulates SOA produced from the irreversible uptake of glyoxal and methylglyoxal by aqueous particles as described in Fu et al. (2008, 2009). Glyoxal and methylglyoxal are two dicarbonyls produced during the oxidation of many biogenic and anthropogenic VOCs, including most importantly isoprene, with minor contributions from acetone, acetylene, alkenes, and aromatics (Fu et al., 2008; Myriokefalitakis et al., 2008). Recent laboratory studies and in situ measurements indicate uptake of glyoxal and methylglyoxal by aqueous particles to form SOA (Schweitzer et al., 1998; Liggio et al., 2005a, b; Volkamer et al., 2007, 2009; Galloway et al., 2009; Sareen et al., 2010; De Haan et al., 2011). We represent this process as a first-order reactive uptake by aqueous aerosols and cloud droplets with a reactive uptake coefficient of $\gamma = 2.9 \times 10^{-3}$, following the chamber study by Liggio et al. (2005) for glyoxal. The same uptake coefficient is adopted for methylglyoxal, consistent with the laboratory results by Zhao et al. (2006). Although uncertainty remains regarding the mechanism of SOA formation by dicarbonyls (Kroll et al., 2005), our model representation provides a state-of-the-science estimate of this secondary OC source. Dicarbonyl SOA is assumed to be fully water-soluble.

Our simulation is conducted from July 2005 to December 2006; the first six months initialize the model. Results from January to December 2006 are analyzed. We also conduct sensitivity tests to by turning off Chinese EC and OC emissions from each of the three source sectors (anthropogenic non-residential, anthropogenic residential,

ACPD
11, 28219–28272, 2011

and biomass burning), in turn and all at once, to evaluate each sector's contribution to surface concentrations, as well as the contribution from non-Chinese sources.

2.2 Bottom-up emission inventories of EC, OC and VOC precursors

As a starting point for our analysis, we use state-of-the-science bottom-up emission inventories for EC, OC, and VOC precursors over China and the rest of East and South Asia to drive our model simulation. Table 1 summarizes the bottom-up emission estimates for Chinese carbonaceous aerosols. Table 2 summarizes the bottom-up Chinese emissions of VOC that are precursors to SOC in our model.

Anthropogenic emissions of EC and OC for China and the rest of East and South Asia are taken from Zhang et al. (2009), developed for the year 2006, including non-residential and residential sources. Non-residential sources include power generation, industry, and transportation. Residential sources include combustion of fossil fuel and biofuel, as well as non-combustive activities. The inventory is based on national and provincial (for China) statistics for the year 2006 or extrapolated statistics from the years 2004 and 2005, then spatially allocated to 0.5° longitude × 0.5° latitude resolution using spatial surrogates. Emission factors are developed using a combination of Chinese measurements, estimates, and data from western sources (Zhang et al., 2007). The estimated anthropogenic non-residential emissions of EC and OC are 0.81 Tg C yr^{-1} and 0.61 Tg C yr^{-1}, respectively, with industry being the largest non-residential source for both EC and OC (mostly from coke and brick production), followed by transportation and power generation. The estimated Chinese residential emissions of EC and OC are 1.00 Tg C yr^{-1} and 2.61 Tg C yr^{-1}, respectively. Total anthropogenic EC emission is 1.81 Tg C yr^{-1} with ±208 % uncertainty (95 % confidence interval). Total anthropogenic OC emission is 3.22 Tg C yr^{-1} with ±258 % uncertainty. Seasonal variations of anthropogenic emissions in China are calculated by assuming a dependence of stove operation on regional monthly mean temperatures for the residential sector, and by using provincial level monthly activity data for the non-residential sector (Zhang et al., 2009). We assume no seasonal variation of anthropogenic emissions outside of China.

ACPD
11, 28219–28272, 2011

Biomass burning emissions of EC and OC for China and rest of East and South Asia are taken from Streets et al. (2003b), which represents average burning activities for the mid-1990s. van der Werf et al. (2010) showed that Chinese biomass burning emission total for the year 2006 is similar to the average annual biomass burning emission total between the years 1997 and 2009 base on satellite observations. We compound the annual biomass burning fluxes with the monthly variation from Duncan et al. (2003), which is based on the Along Track Scanning Radiometer (ATSR) satellite hot spot counts from 1996 to 2000. Total Chinese biomass burning emission of EC is estimated to be 0.11 Tg C yr^{-1}, including 66 % from crop residue, 22 % from grassland, and 12 % from forest. Total Chinese biomass burning emission estimate for OC is 0.71 Tg C yr^{-1}, including 50 % from crop residue, 26 % from forest, and 24 % from grassland. The uncertainties for these estimates are ±450 % (EC) and ±420 % (OC) (Streets et al., 2003b).

Figures 1 and 2 show the spatial distributions of annual EC and OC emissions in the bottom-up inventories. The spatial distributions for EC and OC emissions are very similar in each sector, reflecting their common combustive origin. Non-residential anthropogenic emissions are highest over the heavily industrialized areas of northern China, as well as over the Yangtze River Delta (YRD) and Pearl River Delta (PRD) megacity clusters. Residential emissions are high over densely populated areas, including northern China, Sichuan Basin, Northeastern China Plain, and the YRD and PRD megacity clusters, largely overlapping with industrialized areas. Within China, biomass burning emissions are highest over central and northeastern China from crop residue burning. Outside China, biomass burning emissions are high over the Indochina Peninsula due to land clearing before the local growing season (spring), which can affect the air quality in southern China through transport (Deng et al., 2008).

Table 2 summarizes the emissions of VOC species that are SOC precursors in our model. Biogenic isoprene emissions are calculated with the MEGAN algorithm (Guenther et al., 2006) then scaled to match satellite formaldehyde observations (Fu et al., 2007) to an annual emission of 10.5 Tg yr^{-1}. Biogenic monoterpenes, alcohol, and

ACPD
11, 28219–28272, 2011

sesquiterpene emissions are based on the GEIA inventory (Guenther et al., 1995). Other biogenic VOC precursors include acetone, whose emissions follow Jacob et al. (2002), as well as ethylene and higher alkene emissions, which are scaled to isoprene using emission ratios from Goldstein et al. (1996). Anthropogenic VOC emissions are from the Zhang et al. (2009) inventory described above, with the VOC species mapped to match the GEOS-Chem chemical mechanism. Biomass burning VOC emissions are from Streets et al. (2003b), with alkene, xylenes, and formaldehyde emissions scaled to match satellite constraints (Fu et al., 2007). Biomass burning glyoxal, methylglyoxal, glycolaldehyde, and hydroxyacetone are scaled to biomass burning CO emissions (Streets et al., 2003b) following Fu et al. (2008).

Figure 3 shows the spatial distributions of isoprene, monoterpenes, and toluene emissions. Biogenic VOC are mostly emitted in eastern China reflecting the distribution of vegetation and precipitation. Highest emissions are found over the forested areas in northeastern, central, and southeastern China. Toluene emissions (mostly anthropogenic) are highest over the heavily populated and industrialized North China Plain and Sichuan Basin, as well as over the coastal megacities.

2.3 Carbonaceous aerosol measurements

To constrain the annual sources of carbonaceous aerosols at the country-wide level, we need measurements with sufficient coverage in time and space to allow assessment of seasonal variation and spatial distribution. At the time of this study, there was one carbonaceous aerosol measurement network in China (Zhang et al., 2008), but only one year's worth of data were published and there were gaps in the spatial coverage. Therefore, we compile a database of monthly mean EC and OC surface measurements from previous studies. Our data selection criteria are that the measurements (1) provide information on seasonal variation, (2) combine to cover different parts of China, (3) are analyzed in a consistent manner, and (4) preferably are conducted at background or rural locations to represent regional pollution levels.

ACPD
11, 28219–28272, 2011

Base on the above criteria, we select measurements from five studies conducted between the years 2003 and 2006, including three background sites, seven rural sites, and twenty-one urban sites (Zhang et al., 2008; Qu et al., 2008; Cao et al., 2007, 2009; Y. M. Han et al., 2008). Table 3 lists the details of the measurements. Figure 4 shows the spatial distribution of the measurement sites. Two of these studies (Zhang et al., 2008; Qu et al., 2008) sampled PM_{10} and analyzed EC and OC contents in the same laboratory at the Chinese Academy of Meteorological Sciences. The other three studies sampled $PM_{2.5}$ (Cao et al., 2007; Y. M. Han et al., 2008) or total suspended particles (TSP) (Cao et al., 2009) and analyzed the EC and OC contents at the Institute of Earth Environment, Chinese Academy of Sciences. All analysis followed the IMPROVE (Interagency Monitoring of Protected Visual Environments) thermal/optical reflectance (TOR) protocol (Chow et al., 1993, 2004) using DRI model 2001 Carbon Analyzer. There is therefore some level of consistency and comparability across the measurements. Only EC concentrations at background and rural sites (all sampled as PM_{10} or TSP) will be used in the multiple regression to constrain emissions as described in Sect. 4.

Table 3 summarizes the annual mean surface EC and OC concentrations measured at the 31 background, rural and urban sites. Urban annual mean surface concentrations range from 2.7–14 $\mu g\,C\,m^{-3}$ for EC and 8.2–52 $\mu g\,C\,m^{-3}$ for OC. Rural annual mean surface concentrations range from 2.4–4.7 $\mu g\,C\,m^{-3}$ for EC and 12–40 $\mu g\,C\,m^{-3}$ for OC. These values are significantly higher than the range of annual mean concentrations measured in urban (0.9–1.8 $\mu g\,C\,m^{-3}$ EC, 2.0–5.9 $\mu g\,C\,m^{-3}$ OC) and rural (0.02–1.8 $\mu g\,C\,m^{-3}$ EC, 0.07–7.8 $\mu g\,C\,m^{-3}$ OC) air in North America and in Europe (Hand et al., 2011; Yttri et al., 2007).

3 Model evaluation

We compare simulated surface carbonaceous aerosol concentrations against observations to evaluate our model. In general, model results cannot be evaluated on a

ACPD
11, 28219–28272, 2011

24-h-average basis in continental surface air, because nighttime stratification is often poorly resolved (Jacob et al., 1993). This is not an issue in our case because our model has high vertical resolution near the surface. The situation that our model cannot resolve is where the nighttime Obukhov length is positive and shallower than the bottom model layer (in our case approximately 100 m). We conduct a sensitivity test by suppressing dry deposition when this happens, but find the difference in monthly mean surface concentrations to be less than 5 %. In addition, our top-down emissions (Sect. 4) will be derived using only measurements at non-urban (rural and background) locations, which are generally far from strong surface sources. We will return to the issue of model resolution in Sect. 6.

Figure 5 compares the spatial distributions of observed and simulated surface mean EC and OC concentrations for January and July. Highest concentrations are observed in the densely populated and industrialized areas of northern China, the Sichuan Basin, and the YRD and PRD megacity clusters. Two sites in western China (rural Dunhuang and urban Lasha) show high concentrations in January. Urban sites are consistently more polluted than nearby rural sites, reflecting strong local emissions. At all sites where both January and July measurements are available, EC and OC concentrations are higher in winter than in summer, except at Panyu where the OC concentrations are similar. Although meteorological factors such as boundary layer compression in winter or enhanced wet deposition in summer may lead to such seasonal differences, we find that these effects are small based on the model analysis described below. Instead, stronger anthropogenic emission during the cold months is the main cause for the higher surface concentrations observed in winter.

The simulated EC and OC concentrations show a west-to-east gradient, reflecting the strong emissions in eastern China in the bottom-up inventories, with highest concentrations over northern China and the Sichuan Basin. Model shows higher EC and OC concentrations in winter than in summer, similar to the observations. Understandably, the model is unable to resolve individual urban hotspots. However, the model also underestimates EC and OC concentration at almost all rural sites, particular in January

ACPD
11, 28219–28272, 2011

(with the exception of EC at Taiyangshan). This indicates a region-wide underestimate of carbonaceous aerosol sources associated with anthropogenic activities.

Figures 6 and 7 examine in detail the seasonal variations of surface EC and OC concentrations observed at the ten background and rural sites. At the two background sites in western China, Muztagh Ata and Akdala, EC and OC concentrations are significantly lower than those observed at other Chinese rural sites throughout the year. This indicates that foreign pollution transported from the west is not a significant contributor to the high levels of surface EC and OC observed at interior Chinese sites. Winter, summer, and fall measurements are also low at the Zhuzhang background site in southwestern China. However, data is missing for spring when the impact of transported biomass burning plumes from Southeast Asia to air quality in southern China may be greatest (Deng et al., 2008). Surface concentrations of both EC and OC are higher in fall and winter than in summer at most rural sites (except at Wusumu, where data are available for only four months), again suggesting strong region-wide anthropogenic emissions, likely associated with heating. Both EC and OC concentrations at Dunhuang and Gaolanshan are extremely high and show large enhancements in fall and winter, suggesting that the sites are affected by local anthropogenic activities.

Figure 6 also shows the simulated surface EC concentrations using the bottom-up emission inventories. The simulation reproduces the relatively low concentrations observed at the three background sites. The model agrees well with summertime measurements at Taiyangshan, Jinsha, and Longfengshan, overestimates wintertime measurements at Taiyangshan, but otherwise underestimates observed rural values. Model concentrations are higher in winter than in summer, similar to the observations. Model performance is poorest at Dunhuang and Gaolanshan, where the bottom-up inventories have very little emissions. The average simulated annual mean EC concentration for all rural and background site is 1.1 $\mu g\,C\,m^{-3}$, 56 % lower than the observed 2.5 $\mu g\,C\,m^{-3}$.

We further break down in Fig. 6 the contributions to simulated surface EC concentrations from Chinese anthropogenic residential and non-residential emissions, Chinese

ACPD
11, 28219–28272, 2011

biomass burning emissions, and transport from foreign sources. Contributions from foreign sources are significant only at background sites, in particular at Zhuzhang in spring, which reflects the transport of biomass burning aerosols from Southeast Asia. Chinese biomass burning emissions have distinct seasonal patterns (Duncan et al., 2003; Song et al., 2010), but they have limited impacts at the seven rural sites as simulated by the model. The simulated EC concentrations at all seven rural sites are almost entirely due to Chinese anthropogenic residential and non-residential emissions. Residential emission has the most pronounced seasonal pattern in the model, decreasing rapidly by mid-Spring and rising again in late fall, and it is the main driver for the seasonal variation in the simulated surface EC concentrations. Emissions from the non-residential sector in our model have a mild seasonal variation, and the simulated contributions of that sector likewise do not change much seasonally. Therefore, the observed higher concentrations in winter are unlikely to be due to meteorological factors alone, since these are accounted for in the model. Instead, the observed higher wintertime levels are mainly due to stronger emissions during the cold months, most likely associated with heating.

Figure 7 shows the seasonal variation of simulated surface OC concentrations. Again the model reproduces the low concentrations at background sites. The model severely underestimates measured OC concentrations at all rural sites year-round, except at Taiyangshan from January to March. Moreover, the model fails to reproduce the seasonal pattern at any of the rural sites. Model performance at Dunhuang and Gaolanshan is worse for OC than for EC, particularly during cold months, suggesting that a source associated with a high OC/EC emission ratio is missing in the bottom-up inventories. The average simulated annual mean OC concentration for all rural and background site is 3.4 $\mu g\,C\,m^{-3}$, 76 % lower than the observed 14 $\mu g\,C\,m^{-3}$.

Figure 7 also shows the individual simulated OC components, including OC from primary sectors, semi-volatile SOC, and dicarbonyl SOC. Similar to EC, OC from foreign sources are significant only at the three background sites. Chinese biomass burning constitutes 25 % of the simulated surface OC at Taiyangshan and Jinsha in March,

ACPD
11, 28219–28272, 2011

but otherwise plays a minor role in surface OC concentrations at the rural sites in all seasons. From late fall to early spring, the simulated surface OC concentrations are mainly due to residential emissions. Non-residential emissions are relatively less important to OC than to EC, reflecting the lower OC/EC emission ratio from that sector. The semi-volatile SOC and dicarbonyl SOC sources are comparable in magnitude, with largest production from early summer to early fall, due to the combined effect of higher biogenic precursor emissions and stronger photochemistry in warmer seasons.

Model performance can be summarized by the regression slopes and correlations between model results and observations. Figures 8 and 9 show the scatter plots of simulated versus observed monthly mean surface EC and OC concentrations at rural and background sites for each season. Using the bottom-up inventories, the model underestimates EC observations in all seasons by 35 % to 60 % (reduced major axis regression slopes between 0.40 and 0.65), with correlation coefficients r ranging from 0.41 to 0.48. This shows that there is a real underestimation of EC emissions in the model, not just a misrepresentation in the seasonal variability of emissions. For OC, the simulation using bottom-up inventories severely underestimates observed OC concentrations in all seasons, with regression slopes ranging from 0.16 to 0.51. Moreover, the model cannot capture the observed OC variability; the correlation coefficients r range from 0.08 to 0.26. This indicates that not only are the bottom-up OC emissions too low and spatially and/or temporally misrepresented, but that the representation of secondary formation in the model is also poor. Model performance for OC is best in summer (slope = 0.51), albeit with very poor correlation against observations ($r = 0.26$), because the combined contributions from primary emissions and secondary formation bring the model concentrations closer to observed values. For both EC and OC, the comparison of model results against observations is worst in fall. This may be because the model fails at capturing the timings of the onset of enhanced anthropogenic emissions and/or the shut-down of biogenic SOC formation as the country moves into colder seasons. Also, there may be emission events in fall that are not currently represented in the model, for example, in-field burning of agricultural residues after the fall harvest

ACPD
11, 28219–28272, 2011

(Yang et al., 2008).

Our analyses thus far show that Chinese surface OC concentrations at rural sites are strongly influenced by primary emissions, especially in winter. This is further illustrated in Fig. 10, which shows the correlations between monthly mean OC and EC concentrations in the observation and in the model. Also shown are the reduced-major axis regression lines for OC versus EC measured at urban sites. At urban sites, measured OC and EC are tightly correlated in all seasons due to the overwhelming impact of local primary sources to surface concentrations. Even at rural and background sites, measured OC is still well correlated with EC in all seasons but especially in winter, indicating influence by primary emissions. We further note in Fig. 10 that the measured rural OC versus EC scatter to form "fan-like" patterns, and that the slopes of the lower-right edge of these "fans" are similar to the slopes of the measured urban OC versus EC regression lines. This suggests that Chinese rural and urban sites are affected by the same primary emission activities and thus have similar primary OC/EC emission ratios. The variability of rural OC away from the urban OC versus EC regression line reflects additional secondary production or primary OC sources not represented in the bottom-up inventories (e.g. at Dunhuang and Gaolanshan).

4 "Top-down" estimate of carbonaceous aerosol sources

4.1 EC emission estimates

Based on the model evaluation presented in Sect. 3, we wish to know how the bottom-up EC and OC emissions should be adjusted to best reproduce the magnitude and spatiotemporal patterns of the observations. We use multiple regression to match the simulated EC contributions from each sector against monthly mean observations at the ten rural and background sites. We assume that the simulated EC background (EC from non-Chinese sources) is correct, and subtract it from the observations. The assumption of a correct EC background is valid since the observed EC concentrations

ACPD
11, 28219–28272, 2011

are low at Muztagh Ata and Akdala year-round, as well as at Zhuzhang in summer, fall, and winter, and the model reproduces these low concentrations. As previously mentioned, biomass burning in Southeast Asia in spring may affect air quality in southern China, but measurements are not available at Zhuzhang in spring to constrain this. The multiple regression model is

$$\boldsymbol{c}_{\text{obs}} - \boldsymbol{c}_{\text{background}} = \beta_1 \boldsymbol{c}_{\text{residential}} + \beta_2 \boldsymbol{c}_{\text{non-residential}} + \beta_3 \boldsymbol{c}_{\text{biomass}} + \boldsymbol{\varepsilon}. \quad (1)$$

In Eq. (1), $\boldsymbol{c}_{\text{obs}}$ is the vector of observed monthly mean EC concentrations. $\boldsymbol{c}_{\text{background}}$ is the vector of simulated EC background from non-Chinese sources. $\boldsymbol{c}_{\text{residential}}$, $\boldsymbol{c}_{\text{non-residential}}$, and $\boldsymbol{c}_{\text{biomass}}$ are the vectors of simulated EC contributions from Chinese anthropogenic residential, anthropogenic non-residential, and biomass burning sources, respectively. β_1, β_2, and β_3 are the domain-wide scalar scale factors required for the source sectors to best match the observations as constrained by the multiple regression. $\boldsymbol{\varepsilon}$ is the regression model error vector.

In practice, the contribution from Chinese biomass burning cannot be reliably fitted using available data. This is seen in Fig. 6, where the observations do not reflect the seasonal signatures of biomass burning emissions. We conduct a lack-of-fit F-test and find that including the biomass burning component does not significantly improve the regression. Therefore, we also assume Chinese biomass burning EC emission to be correct and remove its contribution prior to the regression analysis. Since the rural EC measurements mostly reflect the spatiotemporal variability of anthropogenic residential and non-residential sources (Fig. 6), the estimates for these sources are not much affected. The multiple regression gives a scale factor for the anthropogenic residential sector (β_1) of 0.64, with a standard deviation of ±0.49 (bootstrap estimation) and p-value = 0.08. The scale factor for the anthropogenic non-residential sector (β_2) is 2.85, with a standard deviation of ±0.42 and p-value < 0.001. The multiple regression explains 59 % of the observed variance (adjusted $R^2 = 0.59$).

It may seem surprising that the multiple regression indicates reduction of the residential emissions, given that the observations show a stronger wintertime EC enhancement compared to the simulation using bottom-up inventories. This is partly because

ACPD
11, 28219–28272, 2011

the non-residential emissions are also slightly enhanced in winter, such that the combined effect of scaling the two anthropogenic sectors still increases the cold-month emissions in our top-down estimate. More importantly, the distinction between residential and non-residential sources in the multiple regression is somewhat arbitrary, because the spatial patterns of the residential and non-residential emissions are similar (Fig. 1) and not distinguishable with the limited observation data. A better way of understanding the results is that the regression adjusts the EC emissions to best match both the simulated annual mean and the seasonal variability. Thus only the total anthropogenic emission is meaningfully constrained.

Table 1 shows our top-down EC emission estimate. Total anthropogenic emission is 2.94 Tg C yr^{-1}. Adding the unchanged biomass burning emission, the total Chinese EC emissions is 3.05 Tg C yr^{-1}, 59 % larger from the bottom-up estimate. The standard deviation of the top-down EC emission estimate is ±0.78 Tg C yr^{-1}, calculated by combining the top-down uncertainties (standard deviation of the scaling factors from the multiple regression) in quadrature and assuming the bottom-up uncertainty for biomass burning emissions. For comparison with previous bottom-up inventories (Table 1), we calculate the 95 % confidence interval of our top-down emission estimate to be ±50 %. This assumes that the emission estimate probabilities are normally distributed, but the true probabilities are more likely to be lognormally distributed (Streets et al., 2003a).

Figure 1 shows the spatial distribution of the top-down EC emission estimate. Compared to the bottom-up inventories, EC emissions are greatly enhanced in northern and central China, Sichuan basin, and over the YRD and PRD megacity clusters.

4.2 OC emission estimates

Constraining OC emissions from filter-based OC measurements is challenging because it is difficult to separate the primary and secondary OC. One way to circumvent this issue is to estimate OC emissions by scaling EC emissions with OC/EC emission ratios. We experiment with two methods for estimating OC emissions and summarize the results in Table 1. Both methods provide traceability and can easily be recalculated

ACPD
11, 28219–28272, 2011

when updated OC/EC emission ratios become available.

For the first method, we scale the bottom-up anthropogenic OC emissions with the same coefficients β_1 and β_2 obtained from the multiple regression for anthropogenic EC emissions. This is equivalent to applying the OC/EC emission ratios used in the Zhang et al. (2009) bottom-up inventory, and hence can be considered as a "hybrid" approach, combining "bottom-up" statistics with "top-down" observational constraints. The resulting estimates for anthropogenic OC emission is 3.41 Tg C yr^{-1}. Adding the unchanged biomass burning emission estimate of 0.73 Tg C yr^{-1}, the total Chinese OC emission is estimated to be 4.14 Tg C yr^{-1}, only 5 % greater than the bottom-up estimate with very similar spatial distribution (not shown). The uncertainty is similar to that of the bottom-up inventories.

A second, purely "top-down", approach for constraining OC emissions uses the primary OC/EC ratios derived from ambient observations. This method is legitimate because, as argued previously, the distinction between the residential and non-residential components in the EC multiple regression is not robust. Therefore, it is more appropriate to apply an overall primary OC/EC ratio representative of the ambient air mixture. Cao et al. (2007) defined the 20th percentile of observed OC/EC ratio as the primary OC/EC ratio for a particular location in a given season. It is important to distinguish primary OC/EC ratios for different seasons, because the relative strengths of source sectors can change throughout the course of a year. For northern cities (>32° N), they observed primary OC/EC ratios of 2.81 in winter and 1.99 in summer. For southern cities, their observed primary OC/EC ratios are 2.10 in winter and 1.29 in summer. We adopt these values for rural emissions since Fig. 10 shows that rural and urban air are affected by the same primary sources. We use the winter primary OC/EC ratios for April to September and the summer ratios for the rest of the year.

Our top-down estimate for Chinese anthropogenic and biomass burning OC sources are 6.42 Tg C yr^{-1} and 0.25 Tg C yr^{-1}, respectively. Total OC emission is 6.67 Tg C yr^{-1}, 69 % higher than the bottom-up estimate. We calculate the top-down OC uncertainties from the variance of the product of two independent variables (top-down EC emissions

ACPD
11, 28219–28272, 2011

and primary OC/EC ratios) (Goodman, 1960). We use two times the difference between the 20th percentile and the 5th percentile of observed OC/EC ratio from Cao et al. (2007) to represent the standard deviation of primary OC/EC ratio. Uncertainties from each sector are added in quadrature. The resulting overall standard deviation is ±1.30 ($Tg\,C\,yr^{-1}$). The corresponding 95 % confidence interval is calculated as ±38 %, again assuming normality for the emission estimate probabilities.

Figure 2 shows the spatial distributions of top-down OC emissions, which show large enhancements over northern and central China, Sichuan basin, as well as YRD and PRD megacity clusters, similar to the top-down EC emissions.

4.3 Evaluation of the "top-down" emission estimates

Figure 6 shows the simulated EC concentrations at the ten background and rural sites using the top-down EC emission estimates. Using the top-down emission estimates corrects the model low bias at Wusumu, Longfengshan, Jinsha, and LinAn, but the model now overestimates concentrations at Taiyangshan. The adjustments in Chinese emissions have little effect at the background sites. Overall, the simulated average annual mean surface EC concentration at background and rural sites improve to 1.9 $\mu g\,C\,m^{-3}$, in better agreement with observations (2.5 $\mu g\,C\,m^{-3}$). The regression slopes for simulated versus observed EC concentrations greatly improve in all seasons (Fig. 8), with best slope as high as 0.97 in summer, although the correlations are only slightly increased. As shown in Fig. 8, the remaining low bias relative to the observation is mostly due to the underestimation at Dunhuang and Gaolanshan, where emissions are missing in the bottom-up inventories such that applying domain-wide scaling factors do not bring about a great improvement.

Figure 7 shows the model performance for OC at background and rural sites using the hybrid and top-down OC emission estimates. Applying the hybrid OC emission estimates does not lead to improvement in model performance, since it is very similar to the original bottom-up emissions. We will focus on the "pure top-down" OC emission estimates from now on.

ACPD
11, 28219–28272, 2011

Using top-down emission estimates, our simulated OC concentration improve vastly at Taiyangshan, Jinsha, and LinAn, especially in winter. However, the model is still biased low at Dunhuang, Gaolanshan, Wusumu, and Lonfengshan. Overall, the averaged simulated annual mean OC at background and rural sites increase to 5.4 $\mu g\,C\,m^{-3}$, although still 61 % lower than observations (14 $\mu g\,C\,m^{-3}$). As shown in Fig. 9, regression slopes for simulated versus observed OC improve for all seasons, but the model remains unable to capture the variability in the observations. Model low-bias is still worst in fall, either because the model fails to capture the onset of cold-month emissions or misses specific emission events. Neither of these shortcomings can be corrected by applying top-down domain-wide scaling factors.

Figure 11 shows the simulated components of annual mean surface OC using the top-down emission estimates. The national simulated annual mean surface OC is 4.5 $\mu g\,C\,m^{-3}$. Primary anthropogenic emission is the dominant source of surface OC, contributing 3.2 $\mu g\,C\,m^{-3}$ to the Chinese annual mean and accounting for over 60 % of total OC over most of eastern China. Over western China, the simulated contribution of primary anthropogenic emission is generally less than 50 %, although this is likely an underestimation of reality due to missing OC sources in our top-down emission estimates. Primary OC from Chinese biomass burning and non-Chinese sources each contributes less than 0.2 $\mu g\,C\,m^{-3}$ to the national annual mean.

Figure 10 shows the slopes of simulated OC versus EC concentrations in our model using the top-down emission estimates. The slopes of simulated non-urban OC versus EC are brought closer to (1) the slopes of observed OC versus EC at urban sites, and (2) the slopes of the lower-right edge of the data point "fans" formed by observed OC versus EC at non-urban sites. This indicate that the top-down EC and OC emission estimates do a better job than the bottom-up inventories in representing the OC/EC emissions affecting Chinese urban and non-urban air.

Even when using top-down emission estimates, the model is still severely underestimating OC at rural and background sites year-round (Figs. 7 and 9). Excluding Dunhuang and Gaolanshan, we find that the remaining model OC low-bias is not correlated

ACPD
11, 28219–28272, 2011

with observed EC in summer ($r = 0.39$, not significantly different from zero at 5 % significance level, not shown). This suggest that the top-down inventory is capturing most of the primary OC emissions in eastern China in summer, and that the remaining model OC low-bias is likely due to missing SOC in the model. However, the model OC low-bias is significantly correlated with observed EC in eastern China for all other seasons and in western China year-round (not shown), suggesting that the primary OC sources are still too low in our top-down estimate.

5 Contribution of secondary formation to OC

Finally, we quantify the contribution of secondary formation to surface OC. As shown in Fig. 11, semi-volatile SOC and dicarbonyl SOC each contributes 0.5 $\mu g\,C\,m^{-3}$ to the Chinese annual mean surface OC in our model. SOC from both formation pathways are highest over southeastern China, reflecting the combined impact of precursor emissions and photochemical strength. On an annual basis, SOC accounts for 21 % and 19 % of simulated surface OC for the whole of China and in eastern China, respectively. In summer, the simulated secondary fraction of surface OC is 47 % for the whole of China and 45 % in eastern China. This is likely an underestimation, because our simulated OC concentrations are lower than observations (Figs. 7 and 9) in summer. We mentioned previously that the remaining OC differences between the top-down model results and observations at Longfengshan, Taiyangshan, Jinsha, Wusumu, and LinAn in summer are not correlated with observed EC. As an upper estimate, we assume that these remaining OC differences are entirely secondary, thus estimating that 62 % of observed rural surface OC is due to secondary formation in eastern China in summer.

Table 2 summarizes the simulated SOC produced by individual VOC precursors in China. The most important precursor is isoprene, followed by monoterpenes and aromatics, accounting for 39 %, 23 %, and 17 % of total simulated SOC, respectively. In terms of source types, biogenic VOC is the largest source of SOC in our model,

ACPD
11, 28219–28272, 2011

accounting for 70 % of total simulated SOC. Anthropogenic and biomass burning VOC accounts for 24 % and 6 % of total simulated SOC, respectively. Our findings differ from the findings of Z. Han et al. (2008), who found monoterpenes to be the largest sources of SOC in summer in China. This is partly because we use a larger isoprene emission based on satellite formaldehyde observations (Fu et al., 2007). More importantly, we included an additional SOA formation pathway via aqueous uptake of dicarbonyls, of which isoprene is the dominant source. As a result, our simulated SOC concentrations in summer over eastern China are double their simulated values, and our simulated total OC concentrations are in better agreement with observations at the ten rural and background sites.

6 Comparison with previous studies

Table 4 compares our top-down estimates for Chinese anthropogenic carbonaceous aerosol emissions with previous bottom-up inventories for recent years. Previous bottom-up estimates of Chinese anthropogenic emissions range from 0.94 Tg C yr^{-1} to 1.81 Tg C yr^{-1} for EC and from 2.41 Tg C yr^{-1} to 3.84 Tg C yr^{-1} for OC. Our estimates for both EC and OC are at least 60 % larger than all previous bottom-up inventories, but still within the reported range of uncertainties for previous estimates (Streets et al., 2003a; Bond et al., 2007; Zhang et al., 2009; Lamarque et al., 2010; Lei et al., 2011; Lu et al., 2011). In particular, Lu et al. (2011) calculated the 95 % confidence intervals for their emission estimates using Monte Carlo permutation of input parameters in the bottom-up inventory. Our emission estimates for both EC and OC are near the upper limits of their 95 % confidence intervals for the years 2004 and 2008.

Why are previous bottom-up estimates for Chinese carbonaceous aerosol emissions so similarly low? One reason may be because bottom-up inventories are mostly based on activity statistics from the same data sources, such that under-reporting of activity levels and/or over-reporting of emission control implementations would affect all bottom-up estimates in a similar manner. Another reason may be because emission

ACPD
11, 28219–28272, 2011

factors specific to Chinese conditions are scarcely measured. Researchers, out of necessity, adopt middle-of-the-road emission factors from the literature, mostly measured in western societies (Streets et al., 2001, 2003a; Bond et al., 2004; Cao et al., 2006; Ohara et al., 2007; Zhang et al., 2009; Lei et al., 2011; Lu et al., 2011; and references therein). As a result, the median estimates from previous bottom-up inventories are all similarly low, while the associate uncertainties are all similarly large.

Our top-down estimate for OC emission from biomass burning is 0.25 Tg C yr^{-1}, lower than the bottom-up inventory of Streets et al. (2003b). This is because the overall primary OC/EC ratios we adopted from Cao et al. (2007) represent urban air mixtures. Measured OC/EC emission ratios from biomass burning are generally much higher (Andreae and Merlet, 2001), so our estimate is likely to be too low, although measurements are not available to constrain this source in the present study.

Our conclusion that Chinese anthropogenic carbonaceous aerosol emissions are severely underestimated is consistent with the studies of Z. Han et al. (2008) and Koch et al. (2009). Hakami et al. (2005) found anthropogenic EC emissions from northern and northeastern China to be low by a factor of 2 in April 2001, and their derived emissions are consistent with our results. However, they found anthropogenic EC emissions from southeastern China to be overestimated by a factor of 2, inconsistent with our findings. Kondo et al. (2011) measured BC concentration on a remote island in East China Sea and selectively analysed data strongly influenced by transport from China (mostly in spring and winter). They concluded that Chinese annual anthropogenic BC emission is 1.92 Tg C yr^{-1}, similar to the 1.81 Tg C yr^{-1} estimated by Zhang et al. (2009). Both Hakami et al. (2005) and Kondo et al. (2011) used observations far downwind from China during particular seasons, thus may not reflect the total annual emissions from the entire country.

Matsui et al. (2009) simulated EC and OC in northern China in summer 2006 using anthropogenic emissions similar to those estimated by Zhang et al. (2009). They found that their simulated surface EC concentrations were too high at one urban site and one suburban site in Beijing and accordingly concluded that EC emissions are

ACPD
11, 28219–28272, 2011

overestimated around Beijing. Their EC measurements showed a strong diurnal cycle, which they attributed to the accumulation of pollutants near the surface due to nighttime boundary layer compression. They pointed out that a model with coarser vertical resolution would not be able to resolve this nighttime accumulation and would underestimate the 24-h average EC concentrations even if the emissions were correct.

Our purpose in this study is to constrain Chinese annual carbonaceous aerosol sources on a national scale. We make no attempt to resolve urban pollution, which would be strongly influenced by local fluxes. Our top-down emission estimates are derived from rural and background measurements, which are less affected by local emissions and more representative of regional pollutant levels. At Dunhuang and Gaolanshan, where observations are clearly affected by local emissions in winter, the difference between model results and observations are too large to be explained by the coarseness of model resolution alone. Our top-down emission estimates do lead to high biases in summertime EC at a few rural sites, but the overall annual mean performance on a national scale is still much improved compared to that of the bottom-up inventory. This highlights the critical point that top-down emission estimates can only be derived from measurements that fully represent the spatiotemporal variability for the domain and resolution of interest.

7 Conclusions

We simulate carbonaceous aerosols in China and compare model results to surface measurements, with the goal of deriving top-down emission estimates of EC and OC for China, as well as better quantifying the secondary sources of OC. We conduct a year-long simulation, driven by the current Chinese bottom-up emission inventories for EC ($1.92\,\mathrm{Tg\,C\,yr^{-1}}$) and OC ($3.95\,\mathrm{Tg\,C\,yr^{-1}}$). The model contains updated SOC formation mechanisms, including reversible-partitioning of semi-volatile oxidation products from biogenic and anthropogenic VOC precursors, as well as reactive uptake of dicarbonyls on aqueous particles.

ACPD
11, 28219–28272, 2011

A database of surface measurements is compiled from previous studies to represent the spatial and seasonal variability of carbonaceous aerosols in China. Analyses of the observations show that surface EC and OC at Chinese urban and non-urban sites are strongly affected by anthropogenic emissions.

We compare model results to observations at background and rural sites to evaluate the bottom-up inventories. The simulated average annual mean EC concentration for all rural and background sites is 1.1 $\mu g\,C\,m^{-3}$, 56 % lower than the observed 2.5 $\mu g\,C\,m^{-3}$. For OC, the model severely underestimates observed values at all sites year-round, with a simulated average annual mean OC concentration for rural and background sites of 3.4 $\mu g\,C\,m^{-3}$, 76 % lower than the observed 14 $\mu g\,C\,m^{-3}$. Moreover, the model fails to capture the spatiotemporal variability in the OC observations. This indicates that not only are the bottom-up OC emissions too low and spatiotemporally misrepresented, but that the representation of secondary formation in the model is also poor. The model grossly underestimates EC and OC at Dunhuang and Gaolanshan, where an anthropogenic source associated with high OC/EC emission ratio is missing in the bottom-up inventories. Model performances for EC and OC are both worst in fall.

We use multiple regression to derive top-down emission estimates of EC base on monthly observations at rural and background sites. Only the total Chinese anthropogenic emission can be robustly constrained given the available observations. The resulting top-down estimate for Chinese EC emissions is $3.05 \pm 0.78\,Tg\,C\,yr^{-1}$.

We experiment with two approaches for scaling the top-down EC emissions with OC/EC emission ratios to derive OC emission estimates. A "hybrid" approach using the OC/EC emission ratios from the bottom-up inventory of Zhang et al. (2009) yields an estimate of total Chinese OC emission of $4.14\,Tg\,C\,yr^{-1}$, but applying this emission estimate does not significantly improve model performance. A second, purely "top-down", approach uses the primary OC/EC ratios derived from ambient observations by Cao et al. (2007). The resulting top-down estimate for total Chinese OC emission is $6.67 \pm 1.30\,Tg\,C\,yr^{-1}$.

ACPD
11, 28219–28272, 2011

Applying the top-down emission estimates, the simulated average annual mean concentrations at rural and background sites improve to 1.9 $\mu g\,C\,m^{-3}$ (EC) and 5.4 $\mu g\,C\,m^{-3}$ (OC). For EC, the remaining low-bias relative to the observation is mostly due to missing emissions at Dunhuang and Gaolanshan. Even when using the top-down emission estimates, the model is still significantly underestimating observed OC concentrations in all seasons, with little skill in capturing the variability. We find that the top-down inventory is capturing most of the primary OC emissions in eastern China in summer. However, the primary OC sources are still too low in our top-down estimate in eastern China for all other seasons and in western China year-round.

Secondary formation accounts for 21 % of Chinese annual mean surface OC in our model. In summer, as high as 62 % of the observed surface OC may be due to secondary formation in eastern China. SOC produced from semi-volatile compounds and dicarbonyls are comparable in magnitude. The most important SOC precursor is isoprene, followed by monoterpenes and aromatics.

In summary, our analysis points to three shortcomings in the current bottom-up inventories of Chinese carbonaceous aerosols. Firstly, the anthropogenic source is grossly underestimated, particularly for OC, likely due to uncertainties in emissions from small industries, residential combustion, and transportation (Zhang et al., 2009; Lu et al., 2011). Secondly, there is a missing source in western China, characterized by a high OC/EC emission ratio and a strong enhancement during the colder months, likely associated with the use of biofuels or other low-quality fuels for heating. The third issue is that sources in fall are not well represented, either because the seasonal shifting of emissions and/or secondary formation is poorly captured or because specific fall emission events are missing. In addition, the seasonal contributions from biomass burning in China and in Southeast Asia may also be underestimated, but measurements are not available to constrain these sources in this study.

Our top-down EC and OC emission estimates are at least 60 % higher than all previous bottom-up estimates. Two questions arise. The first question is why are all previous bottom-up estimates so similarly low? We speculate that the use of activity

ACPD
11, 28219–28272, 2011

statics from the same data sources and the adoption of emission factors from the literature may be the cause. The second question is whether our emission estimates are supported by other observations? Our results are consistent with the findings from a few previous seasonal studies. We plan to explore the use of other data, such as satellite aerosol optical depth observations, to evaluate our results. Many gaps remain in our understanding of Chinese carbonaceous aerosol sources. More regional measurements with better spatiotemporal coverage, especially over western China, are needed to address these gaps.

Acknowledgements. This work is funded by the Hong Kong Research Grant Council (PolyU 5175/09E) and by Peking University. We thank Shuhua Liu and Hongsheng Zhang for helpful discussions.

References

Andreae, M. O. and Merlet, P.: Emission of trace gases and aerosols from biomass burning, Global Biogeochem. Cy., 15, 955–966, doi:10.1029/2000GB001382, 2001.

Bey, I., Jacob, D. J., Yantosca, R. M., Logan, J. A., Field, B., Fiore, A. M., Li, Q., Liu, H., Mickley, L. J., and Schultz, M.: Global modeling of tropospheric chemistry with assimilated meteorology: model description and evaluation, J. Geophys. Res., 106, 23073–23096, 2001.

Bond, T. C., Streets, D. G., Yarber, K. F., Nelson, S. M., Woo, J.-H., and Klimont, Z.: A technology-based global inventory of black and organic carbon emissions from combustion, J. Geophys. Res., 109, D14203, doi:10.1029/2003JD003697, 2004.

Bond, T. C., Bhardwaj, E., Dong, R., Jogani, R., Jung, S., Roden, C., Streets, D. G., and Trautmann, N. M.: Historical emissions of black and organic carbon aerosol from energy-related combustion, Global Biogeochem. Cy., 21, GB2018, doi:10.1029/2006GB002840, 2007.

Cao, G., Zhang, X., and Zheng, F.: Inventory of black carbon and organic carbon emissions from China, Atmos. Environ., 40, 6516–6527, doi:10.1016/j.atmosenv.2006.05.070, 2006.

Cao, J. J., Lee, S. C., Chow, J. C. Watson, J. G., Ho, K. F., Zhang, R. J., Jin, Z. D., Shen, Z. X., Chen, G. C., Kang, Y. M., Zou, S. C., Zhang, L. Z., Qi, S. H., Dai, M. H., Cheng, Y., and Hu, K.: Spatial and seasonal distributions of carbonaceous aerosols over China, J. Geophys. Res., 112, D22S11, doi:10.1029/2006JD008205, 2007.

ACPD
11, 28219–28272, 2011

Cao, J. J., Xu, B. Q., He, J. Q., Liu, X. Q., Han, Y. M., Wang, G. H., and Zhu, C. S.: Concentrations, seasonal variations, and transport of carbonaceous aerosol at a remote Mountainous region in western China, Atmos. Environ., 43, 4444–4452, doi:10.1016/j.atmosenv.2009.06.023, 2009.

Carlton, A. G., Wiedinmyer, C., and Kroll, J. H.: A review of Secondary Organic Aerosol (SOA) formation from isoprene, Atmos. Chem. Phys., 9, 4987–5005, doi:10.5194/acp-9-4987-2009, 2009.

Chen, D., Wang, Y., McElroy, M. B., He, K., Yantosca, R. M., and Le Sager, P.: Regional CO pollution and export in China simulated by the high-resolution nested-grid GEOS-Chem model, Atmos. Chem. Phys., 9, 3825–3839, doi:10.5194/acp-9-3825-2009, 2009.

Cooke, W. F., Liousse, C., Cachier, H., and Feichter, J.: Construction of a 1°×1° fossil fuel emission data set for carbonaceous aerosol and implementation and radiative impact in the ECHAM-4 model, J. Geophys. Res., 104, 22137–22162, 1999.

Chow, J. C., Watson, J. G., Pritchett, L. C., Pierson, W. R., Frazier, C. A., and Purcell, P. G.: The DRI thermal/optical reflectance carbon analysis system: Description, evaluation and applications in US air quality studies, Atmos. Environ., Part A, 27, 1185–1201, 1993.

Chow, J. C., Watson, J. G., Chen, L.-W. A., Arnott, W. P., Moosmüller, H., and Fung, K. K.: Equivalence of elemental carbon by thermal/optical reflectance and transmittance with different temperature protocols, Environ. Sci. Technol., 38, 4414–4422, 2004.

Chung, S. H. and Seinfeld, J. H.: Global distribution and climate forcing of carbonaceous aerosols, J. Geophys. Res., 107, 4407, doi:10.1029/2001JD001397, 2002.

Cooke, W. F., Liousse, C., Cachier, H., and Feichter, J.: Construction of a 1°×1° fossil fuel emission data set for carbonaceous aerosol and implementation and radiative impact in the ECHAM-4 model, J. Geophys. Res., 104, 22137–22162, 1999.

De Haan, D. O., Hawkins, L. N., Kononenko, J. A., Turley, J. J., Corrigan, A. L., Tolbert, M. A., and Jimenez, J. L.: Formation of nitrogen-containing oligomers by methylglyoxal and amines in simulated evaporating cloud droplets, Environ. Sci. Tech., 45, 984–991, doi:10.1021/es102933x, 2011.

Deng, X., Tie, X., Zhou, X., Wu, D., Zhong, L., Tan, H., Li, F., Huang, X., Bi, X., and Deng, T.: Effects of Southeast Asia biomass burning on aerosols and ozone concentrations over the Pearl River Delta (PRD) Region, Atmos. Env., 42, 8493–8501, doi:10.1016/j.atmosenv.2008.08.013, 2008.

Fu, T.-M., Jacob, D. J., Palmer, P. I., Chance, K., Wang, Y. X., Barletta, B., Blake, D. R.,

ACPD
11, 28219–28272, 2011

Stanton, J. C., and Pilling, M. J.: Spaced-based formaldehyde measurements as constraints on volatile organic compound emissions in east and south Asia and implications for ozone, J. Geophys. Res., 112, D06312, doi:10.1029/2006JD007853, 2007.

Fu, T.-M., Jacob, D. J., Wittrock, F., Burrows, J. P., Vrekoussis, M., and Henze, D. K.: Global budgets of atmospheric glyoxal and methylglyoxal, and implications for formation of secondary organic aerosols, J. Geophys. Res., 113, D15303, doi:10.1029/2007JD009505, 2008.

Fu, T.-M., Jacob, D. J., and Heald, C. L.: Aqueous-phase reactive uptake of dicarbonyls as a source of organic aerosol over eastern North America, Atmos. Environ., 43, 1814–1822, doi:10.1016/j.atmosenv.2008.12.029, 2009.

Galloway, M. M., Chhabra, P. S., Chan, A. W. H., Surratt, J. D., Flagan, R. C., Seinfeld, J. H., and Keutsch, F. N.: Glyoxal uptake on ammonium sulphate seed aerosol: reaction products and reversibility of uptake under dark and irradiated conditions, Atmos. Chem. Phys., 9, 3331–3345, doi:10.5194/acp-9-3331-2009, 2009.

Goldstein, A. H., Fan, S. M., Goulden, M. L., Munger, J. W., and Wofsy, S. C.: Emissions of ethane, propene, and 1-butene by a midlatitude forest, J. Geophys., Res., 101, 9149–9157, 1996.

Goodman, L. A.: On the exact variance of products, J. American. Stat. Assoc., 55, 708–713, 1960.

Guenther, A., Hewitt, C. N., Erickson, D., Fall, R., Geron, C., Graedel, T., Harley, P., Klinger, L., Lerdau, M., McKay, W., Pierce, T., Scholes, B., Steinbrecher, R., Tallamraju, R., Taylor, J., and Zimmerman, P.: A global model of natural volatile organic compound emissions, J. Geophys. Res., 100, 8873–8892, 1995.

Guenther, A., Karl, T., Harley, P., Wiedinmyer, C., Palmer, P. I., and Geron, C.: Estimates of global terrestrial isoprene emissions using MEGAN (Model of Emissions of Gases and Aerosols from Nature), Atmos. Chem. Phys., 6, 3181–3210, doi:10.5194/acp-6-3181-2006, 2006.

Hakami, A., Henze, D. K., Seinfeld, J. H., Chai, T., Tang, Y., Carmichael, G. R., and Sandu, A.: Adjoint inverse modeling of black carbon during the Asian Pacific Regional Aerosol Characterization Experiment, J. Geophys. Res., 110, D14301, doi:10.1029/2004JD005671, 2005.

Hallquist, M., Wenger, J. C., Baltensperger, U., Rudich, Y., Simpson, D., Claeys, M., Dommen, J., Donahue, N. M., George, C., Goldstein, A. H., Hamilton, J. F., Herrmann, H., Hoffmann, T., Iinuma, Y., Jang, M., Jenkin, M. E., Jimenez, J. L., Kiendler-Scharr, A., Maenhaut, W.,

ACPD
11, 28219–28272, 2011

McFiggans, G., Mentel, Th. F., Monod, A., Prévôt, A. S. H., Seinfeld, J. H., Surratt, J. D., Szmigielski, R., and Wildt, J.: The formation, properties and impact of secondary organic aerosol: current and emerging issues, Atmos. Chem. Phys., 9, 5155–5236, doi:10.5194/acp-9-5155-2009, 2009.

Han, Y. M., Han, Z. W., Cao J. J., Chow, J. C., Watson, J. G., An, Z. S., Liu, S. X., and Zhang, R. J.: Distribution and origin of carbonaceous aerosol over a rural high-mountain lake area, Northern China and its transport significance, Atmos. Environ., 42, 2405–2414, doi:10.1016/j.atmosenv.2007.12.020, 2008.

Han, Z., Zhang, R., Wang, Q., Wang, W., Cao, J., and Xu, J.: Regional modeling of organic aerosols over China in summertime, J. Geophys. Res., 113, D11202, doi:10.1029/2007JD009436, 2008.

Hand, J. L., Copeland, S. A., Day, D. E., Dillner, A. M., Indresand, H., Malm, W. C., McDade, C. E., Moore Jr., C. T., Pitchford, M. L., Schichtel, B. A., and Watson, J. G.: IMPROVE (Interagency Monitoring of Protected Visual Environments): Spatial and seasonal patterns and temporal variability of haze and its constituents in the United States, Report V, CIRA Report ISSN: 0737-5352-87, Colo. State Univ., Fort Collins, 2011.

Henze, D. K. and Seinfeld, J. H.: Global secondary organic aerosol from isoprene oxidation, Geophys. Res. Lett., 33, L09812, doi:10.1029/2006GL025976, 2006.

Henze, D. K., Seinfeld, J. H., Ng, N. L., Kroll, J. H., Fu, T.-M., Jacob, D. J., and Heald, C. L.: Global modeling of secondary organic aerosol formation from aromatic hydrocarbons: high- vs. low-yield pathways, Atmos. Chem. Phys., 8, 2405–2420, doi:10.5194/acp-8-2405-2008, 2008.

Herndon, S. C., Onasch, T. B., Wood, E. C., Kroll, J. H., Canagaratna, M. R., Jayne, J. T., Zavala, M. A., Knighton, W. B., Mazzoleni, C., Dubey, M. K., Ulbrich, I. M., Jimenez, J. L., Seila, R., de Gouw, J. A., de Foy, B., Fast, J., Molina, L. T., Kolb, C. E., and Worsnop, D. R.: Correlation of secondary organic aerosol with odd oxygen in Mexico City, Geophys. Res. Lett., 35, L15804, doi:10.1029/2008GL034058, 2008.

Jeong, C.-H., Hopke, P. K., Kim, E., and Lee, D.-W.: The comparison between thermal-optical transmittance elemental carbon and aethalometer black carbon measured at multiple monitoring sites, Atmos. Environ., 38, 5193–5204, doi:10.1016/j.atmosenv.2004.02.065, 2004.

Kondo, Y., Oshima, N., Kajino, M., Mikami, R., Moteki, N., Takegawa, N., Verma, R., Kajii, Y., Kato, S., and Takami, A.: Emissions of black carbon in East Asia estimated from observations at a remote site in the East China Sea, J. Geophys. Res., 116, D16201,

ACPD
11, 28219–28272, 2011

doi:10.1029/2011JD015637, 2011.
Lamarque, J.-F., Bond, T. C., Eyring, V., Granier, C., Heil, A., Klimont, Z., Lee, D., Liousse, C., Mieville, A., Owen, B., Schultz, M. G., Shindell, D., Smith, S. J., Stehfest, E., Van Aardenne, J., Cooper, O. R., Kainuma, M., Mahowald, N., McConnell, J. R., Naik, V., Riahi, K., and van Vuuren, D. P.: Historical (1850–2000) gridded anthropogenic and biomass burning emissions of reactive gases and aerosols: methodology and application, Atmos. Chem. Phys., 10, 7017–7039, doi:10.5194/acp-10-7017-2010, 2010.
Lei, Y., Zhang, Q., He, K. B., and Streets, D. G.: Primary anthropogenic aerosol emission trends for China, 1990–2005, Atmos. Chem. Phys., 11, 931–954, doi:10.5194/acp-11-931-2011, 2011.
Liao, H., Henze, D. K., Seinfeld, J. H., Wu, S., and Mickley, L. J.: Biogenic secondary organic aerosol over the United States: comparison of climatological simulations with observations, J. Geophys. Res., 112, D06201, doi:10.1029/2006JD007813, 2007.
Liggio, J., Li, S.-M., and McLaren, R.: Reactive uptake of glyoxal by particulate matter, J. Geophys. Res., 110, D10304, doi:10.1029/2004JD005113, 2005.
Liu, H., Jacob, D. J., Bey, I., and Yantosca, R. M.: Constraints from 210Pb and 7Be on wet deposition and transport in a global three-dimensional chemical tracer model driven by assimilated meteorological fields, J. Geophys. Res., 106, 12109–12128, 2001.
Liu, H., Zhang, L., and Wu, J.: A modeling study of the climate effects of sulfate and carbonaceous aerosols over China, Adv. Atmos. Sci., 27, 1276–1288, doi:10.1007/s00376-010-9188-y, 2010.
Lu, Z., Zhang, Q., and Streets, D. G.: Sulfur dioxide and primary carbonaceous aerosol emissions in China and India, 1996–2010, Atmos. Chem. Phys., 11, 9839–9864, doi:10.5194/acp-11-9839-2011, 2011.
Malm, W. C., Sisler, J. F., Huffman, D., Eldred, R. A., and Cahill, T. A.: Spatial and seasonal trends in particle concentration and optical extinction in the United States, J. Geophys. Res., 99, 1347–1370, doi:10.1029/93JD02916, 1994.
Mari, C., Jacob, D. J., and Bechtold, P.: Transport and scavenging of soluble gases in a deep convective cloud, J. Geophys. Res., 105, 22255–22267, 2000.
Matsui, H., Koike, M., Kondo, Y., Takegawa, N., Kita, K., Miyazaki, Y., Hu, M., Chang, S.-Y., Blake, D. R., Fast, J. D., Zaveri, R. A., Streets, D. G., Zhang, Q., and Zhu, T.: Spatial and temporal variations of aerosols around Beijing in summer 2006: Model evaluation and source apportionment, J. Geophys. Res., 114, D00G13, doi:10.1029/2008JD010906, 2009.

ACPD
11, 28219–28272, 2011

Myriokefalitakis, S., Vrekoussis, M., Tsigaridis, K., Wittrock, F., Richter, A., Brühl, C., Volkamer, R., Burrows, J. P., and Kanakidou, M.: The influence of natural and anthropogenic secondary sources on the glyoxal global distribution, Atmos. Chem. Phys., 8, 4965–4981, doi:10.5194/acp-8-4965-2008, 2008.

Odum, J. R., Hoffmann, T., Bowman, F., Collins, D., Flagan, R. C., and Seinfeld, J. H.: Gas/particle partitioning and secondary organic aerosol yields, Environ. Sci. Tech., 30, 2580–2585, 1996.

Pankow, J. F.: An absorption model of gas/particle partitioning of organic compounds in the atmosphere, Atmos. Environ., 28, 185–188, 1994a.

Pankow, J. F.: An absorption model of gas/particle partitioning involved in the formation of secondary organic aerosol, Atmos. Environ., 28, 189–193, 1994b.

Park, R. J., Jacob, D. J., Chin, M., and Martin, R. V.: Sources of carbonaceous aerosols over the United States and implications for natural visibility, J. Geophys. Res., 108, 4355, doi:10.1029/2002JD003190, 2003.

Park, R. J., Jacob, D. J., Palmer, P. I., Clarke, A. D., Weber, R. J., Zondlo, M. A., Eisele, F. L., Bandy, A. R., Thornton, D. C., Sachse, G. W., and Bond, T. C.: Export efficiency of black carbon aerosol in continental outflow: global implications, J. Geophys. Res., 110, D11205, doi:10.1029/2004JD005432, 2005.

Qu, W. J., Zhang, X. Y., Arimoto, R., Wang, D., Wang, Y. Q., Yan, L. W., and Li, Y.: Chemical composition of the background aerosol at two sites in southwestern and northwestern China: potential influences of regional transport, Tellus, 60B, 657–673, doi:10.1111/j.1600-0889.2008.00342.x, 2008.

Sareen, N., Schwier, A. N., Shapiro, E. L., Mitroo, D., and McNeill, V. F.: Secondary organic material formed by methylglyoxal in aqueous aerosol mimics, Atmos. Chem. Phys., 10, 997–1016, doi:10.5194/acp-10-997-2010, 2010.

Song, Y., Chang, D., Liu, B., Miao, W., Zhu, L., and Zhang, Y.: A new emission inventory for nonagricultural open fires in Asia from 2000 to 2009, Environ. Res. Lett., 5, 014014, doi:10.1088/1748-9326/5/1/014014, 2010.

Streets, D. G., Gupta, S., Waldhoff, S. T., Wang, M. Q., Bond, T. C., and Bo, Y.: Black carbon emissions in China, Atmos. Environ., 35, 4281–4296, 2001.

Streets, D. G., Bond, T. C., Carmichael, G. R., Fernandes, S. D., Fu, Q., He, D., Klimont, Z., Nelson, S. M., Tsai, N. Y., Wang, M. Q., Woo, J.-H., and Yarber, K. F.: An inventory of gaseous and primary aerosol emissions in Asia in the year 2000, J. Geophys. Res., 108,

ACPD
11, 28219–28272, 2011

8809, doi:10.1029/2002JD003093, 2003a.
Streets, D. G., Yarber, K. F., Woo, J.-H., and Carmichael, G. R.: Biomass burning in Asia: Annual and seasonal estimates and atmospheric emissions, Global Biogeochem. Cy., 17, 1099, doi:10.1029/2003GB002040, 2003b.
Turpin, B. J. and Lim, H. J.: Species contributions to $PM_{2.5}$ mass concentrations: Revisiting common assumptions for estimating organic mass, Aerosol. Sci. Tech., 35, 602–610, 2001.
van der Werf, G. R., Randerson, J. T., Giglio, L., Collatz, G. J., Mu, M., Kasibhatla, P. S., Morton, D. C., DeFries, R. S., Jin, Y., and van Leeuwen, T. T.: Global fire emissions and the contribution of deforestation, savanna, forest, agricultural, and peat fires (1997–2009), Atmos. Chem. Phys., 10, 11707–11735, doi:10.5194/acp-10-11707-2010, 2010.
Volkamer, R., Platt, U., and Wirtz, K.: Primary and secondary glyoxal formation from aromatics: experimental evidence for the bicycloalkyl-radical pathway from benzene, toluene, and p-xylene, J. Phys. Chem. A, 105, 7865–7874, 2001.
Wang, X. M., Wu, Z. Y., and Liang, G. X.: WRF/CHEM modeling of impacts of weather conditions modified by Urban expansion on secondary organic aerosol formation over Pearl River Delta, Particuology, 7, 384–391, doi:10.1016/j.partic.2009.04.007, 2009.
Wang, Y., Jacob, D. J. and Logan, J. A.: Global simulation of tropospheric O_3-NO_x-hydrocarbon chemistry: 1. Model formulation, J. Geophys. Res., 103, 10713–10726, 1998.
Wang, Y., Hao, J., McElroy, M. B., Munger, J. W., Ma, H., Chen, D., and Nielsen, C. P.: Ozone air quality during the 2008 Beijing Olympics: effectiveness of emission restrictions, Atmos. Chem. Phys., 9, 5237–5251, doi:10.5194/acp-9-5237-2009, 2009.
Wang, Y. X., McElroy, M. B., Jacob, D. J., and Yantosca, R. M.: A nested grid formulation for chemical transport over Asia: applications to CO, J. Geophys. Res., 109, D22307, doi:10.1029/2004jd005237, 2004.
Wesely, M. L.: Parameterization of surface resistance to gaseous dry deposition in regional-scale numerical models, Atmos. Environ., 23, 1293–1304, 1989.
Yang, S., He, H., Lu, S., Chen, D., and Zhu, J.: Quantification of crop residue burning in the field and its influence on ambient air quality in Suqian, China, Atmos. Environ., 42, 1961–1969, doi:10.1016/j.atmosenv.2007.12.007, 2008.
Yttri, K. E., Aas, W., Bjerke, A., Cape, J. N., Cavalli, F., Ceburnis, D., Dye, C., Emblico, L., Facchini, M. C., Forster, C., Hanssen, J. E., Hansson, H. C., Jennings, S. G., Maenhaut, W., Putaud, J. P., and Tørseth, K.: Elemental and organic carbon in PM_{10}: a one year measurement campaign within the European Monitoring and Evaluation Programme EMEP,

ACPD
11, 28219–28272, 2011

Atmos. Chem. Phys., 7, 5711–5725, doi:10.5194/acp-7-5711-2007, 2007.
Zhao, J., Levitt, N. P., Zhang, R., and Chen, J.: Heteorogeneous reactions of methylglyoxal in acidic media: implications for secondary organic aerosol formation, Environ. Sci. Technol., 40, 7682–7687, doi:10.1021/es060610k, 2006.
Zhang, Q., Streets, D. G., He, K., and Klimont, Z.: Major componenets of China's anthropogenic primary particulate emissions, Environ. Res. Lett., 2, 045027, doi:10.1088/1748-9326/2/4/045027, 2007.
Zhang, Q., Streets, D. G., Carmichael, G. R., He, K. B., Huo, H., Kannari, A., Klimont, Z., Park, I. S., Reddy, S., Fu, J. S., Chen, D., Duan, L., Lei, Y., Wang, L. T., and Yao, Z. L.: Asian emissions in 2006 for the NASA INTEX-B mission, Atmos. Chem. Phys., 9, 5131–5153, doi:10.5194/acp-9-5131-2009, 2009.
Zhang, X. Y., Wang, Y. Q., Wang, D., Gong, S. L., Arimoto, R., Mao, L. J., and Li, J.: Characterization and sources of regional-scale transported carbonaceous and dust aerosols from different pathways in costal and sandy land areas of China. J. Geophy. Res. 110, D15301, doi:10.1029/2004JD005457, 2005.
Zhang, X. Y., Wang, Y. Q., Zhang, X. C., Guo, W., Gong, S. L., Zhao, P., and Jin, J. L.: Carbonaceous aerosol composition over various regions of China during 2006, J. Geophys. Res., 113, D14111, doi:10.1029/2007JD009525, 2008.
Zhou, X., Gao, J., Wang, T., Wu, W., and Wang, W.: Measurement of black carbon aerosols near two Chinese megacities and the implications for improving emission inventories, Atmos. Environ., 43, 3918–3924, doi:10.1016/j.atmosenv.2009.04.062, 2009.

ACPD
11, 28219–28272, 2011

Table 1. Chinese carbonaceous aerosol emission estimates.

Source sectors	EC ($Tg\,C\,yr^{-1}$)		OC ($Tg\,C\,yr^{-1}$)		
	Bottom-up	Top-down	Bottom-up	Hybrid[e]	Top-down
Anthropogenic		2.94 ± 0.60 (±40 %)[c]		3.41	6.42 ± 1.10 (±34 %)[c]
non-residential	0.81[a]		0.61[a]		
residential	1.00[a]		2.61[a]		
Biomass burning	0.11[b]	0.11 ± 0.50 (±450 %)[d]	0.73[b]	0.73[d]	0.25 ± 0.69 (±540 %)[c]
China total	1.92	3.05 ± 0.78 (±50 %)[c]	3.95	4.14	6.67 ± 1.30 (±38 %)[c]

[a] From Zhang et al. (2009). Uncertainties, represented as 95 % confidence intervals (CI), are ±208 % for EC and ±258 % for OC.
[b] From Streets et al. (2003b). Uncertainties, represented as 95 % CI, are ±450 % for EC and ±420 % for OC.
[c] Uncertainties are represented as ± standard deviations. The corresponding 95 % CI are calculated assuming normal distribution and are shown in parentheses. See text for details.
[d] Bottom-up emissions and uncertainties are adopted since observational constraints are not available.
[e] Uncertainties are not calculated but are expected to be similar to those of the bottom-up emissions.

ACPD
11, 28219–28272, 2011

Table 2. Volatile organic compound (VOC) precursors of secondary organic carbon aerosols (SOC) in China.

VOC precursor	Chinese emission[a] ($Tg\,yr^{-1}$)				Simulated contribution to annual mean surface OC concentration in China[b] ($\mu g\,C\,m^{-3}$)		
	Anthropogenic[c]	Biomass burning	Biogenic	Total	Semi-volatile SOC	Dicarbonyl SOC[d]	Total SOC
Isoprene	–	–	10.5	10.5	0.10	0.29	0.39
Monoterpenes	–	–	5.6	5.6	0.21	0.01	0.23
Aromatics[e]	5.3	0.11	–	5.4	0.09	0.08	0.17
Ethylene	2.2	1.6	0.2	4.1	–	0.04	0.04
Sesquiterpenes	–	–	0.6	0.6	0.04	–	0.04
Alcohols	–	–	1.6	1.6	0.03	–	0.03
$\geq C_4$ alkanes	4.8	0.1	–	4.8	–	0.02	0.02
Acetylene	2.4	0.1	–	2.5	–	0.02	0.02
Acetone	0.2	0.3	1.6	2.1	–	0.02	0.02
$\geq C_3$ alkenes	0.6	1.7	0.3	2.6	–	0.01	0.01
Glyoxal	–	0.2	–	0.2	–	0.01	0.01
Methylglyoxal	–	0.1	–	0.1	–	0.01	0.01
Hydroxyacetone	–	0.1	–	0.1	–	0.006	0.006
Propane	0.4	0.1	–	0.5	–	0.005	0.005
Glycolaldehyde	–	0.2	–	0.2	–	0.001	0.001
Total	15.9	4.6	20.4	40.9	0.48	0.53	1.01

[a] Represents primary emissions only.
[b] From GEOS-Chem simulation using the top-down EC and OC emission estimates described in the text.
[c] Includes anthropogenic residential and non-residential sources
[d] Relative contributions to dicarbonyl SOC from individual VOC precursors are estimated using dicarbonyl molar yields calculated by Fu et al. (2007) based on a one-year GEOS-Chem global simulation.
[e] Includes benzene, toluene, and xylenes.

ACPD
11, 28219–28272, 2011

Table 3. List of Chinese surface EC and OC concentration observations used in this study.

Site[a]	Aerosol size sampled[b]	Filter accumulation period/sampling frequency	Observation period	Observed annual mean EC/OC surface concentrations[c] ($\mu g\,C\,m^{-3}$)	Simulated annual mean EC/OC surface concentrations[d] ($\mu g\,C\,m^{-3}$)		Used in multiple regression to constrain EC emissions?	Reference[e]
					using "bottom-up" emission inventories[d]	using "top-down" emission estimates		
Background								
Akdala (47.1° N, 87.97° E)	PM_{10}	72 h/every 3–10 days	Aug, Sep, Nov, and Dec 2004; Jan–Mar 2005	0.33/2.8	0.23/0.78	0.23/0.83	Yes	(1)
Muztagh Ata (38.3° N, 75.01° E)	TSP	~7 days[f]/weekly	2005[g]	0.051/0.51	0.093/0.49	0.10/0.47	Yes	(2)
Zhuzhang (28° N, 99.72° E)	PM_{10}	72 h/every 3–4 days	Aug–Dec 2004; Jan–Feb 2005	0.35/3.1	0.15/1.1	0.18/0.98	Yes	(1)
Rural								
Dunhuang (40.15° N, 94.68° E)	PM_{10}	24 h/every 3 days	2006	4.1/29	0.19/0.88	0.22/0.82	Yes	(3)
Gaolanshan (36° N, 105.85° E)	PM_{10}	24 h/every 3 days	2006	3.7/18	1.0/2.7	1.3/4.1	Yes	(3)
Wusumu (40.56° N, 112.55°E)	PM_{10}	24 h/daily	Sep 2005; Jan and Jul 2006; May 2007	3.7/27	1.8/4.3	3.2/8.9	Yes	(4)
Longfengshan (44.73°N, 127.6° E)	PM_{10}	24 h/every 3 days	2006	2.4/16	1.6/4.7	2.3/7.4	Yes	(3)
Taiyangshan (29.17° N, 111.71° E)	PM_{10}	24 h/every 3 days	2006	2.4/12	2.5/7.5	3.9/11	Yes	(3)
Jinsha (29.63° N, 114.2° E)	PM_{10}	24 h/every 3 days	Jun–Nov 2006	3.0/14	1.9/6.8	3.5/10	Yes	(3)
LinAn (30.3° N, 119.73° E)	PM_{10}	24 h/every 3 days	2004-2005	4.8/15	2.0/4.9	4.1/9.4	Yes	(3)
Urban								
Jinchang (38.3° N, 101.1° E)	$PM_{2.5}$	24 h/daily	Jan, Jul, and Aug 2003	3.4/16	0.40/1.5	0.43/1.6	No	(5)
Yulin (38.3° N, 109.8° E)	$PM_{2.5}$	24 h/daily	Jan, Jul, and Aug 2003	6.2/24	1.4/4.4	1.8/6.2	No	(5)
Gucheng[h] (39.13° N, 115.8° E)	PM_{10}	24 h/every 3 days	2006	12/40	4.9/9.0	8.1/22	No	(3)
Beijing (39.9° N, 116.4° E)	$PM_{2.5}$	24 h/daily	Jan and Jul 2003	6.2/23	6.9/13	9.3/27	No	(5)

ACPD
11, 28219–28272, 2011

Table 3. Continued.

Site[a]	Aerosol size sampled[b]	Filter accumulation period/sampling frequency	Observation period	Observed annual mean EC/OC surface concentrations[c] ($\mu g\,C\,m^{-3}$)	Simulated annual mean EC/OC surface concentrations[d] ($\mu g\,C\,m^{-3}$)		Used in multiple regression to constrain EC emissions?	Reference[e]
					using "bottom-up" emission inventories[d]	using "top-down" emission estimates		
Tianjin (39.1° N, 117.2° E)	$PM_{2.5}$	24 h/daily	Jan and Jul 2003	6.1/28	4.5/8.9	7.0/20	No	(5)
Dalian (38.9° N, 121.63° E)	PM_{10}	24 h/every 3 days	2006	5.4/18	1.5/4.1	2.4/7.2	No	(3)
Changchun (43.9° N, 125.3° E)	$PM_{2.5}$	24 h / daily	Jan, Jul, and Aug 2003	8.2/26	3.2/7.0	4.7/14	No	(5)
XiAn (34.43° N, 108.97° E)	PM_{10}	24 h/every 3 days	Jan-Aug 2006; Oct-Dec 2006	14/42	2.9/6.1	4.7/14	No	(3)
Zhengzhou (34.78° N, 113.68° E)	PM_{10}	24 h/every 3 days	Jan–Aug 2006	9.5/25	4.7/10	7.8/21	No	(3)
Qingdao (36° N, 120.3° E)	$PM_{2.5}$	24 h/daily	Jan and Jul 2003	3.9/16	1.9/4.7	3.0/8.5	No	(5)
Lhasa (29.67° N, 91.13° E)	PM_{10}	24 h/every 3 days	2006	3.7/21	0.20/1.1	0.20/0.97	No	(3)
Chengdu (30.65° N, 104.03° E)	PM_{10}	24 h/every 3 days	2006	11/33	2.7/7.0	3.8/8.5	No	(3)
Chongqing (29.5° N, 106.5° E)	$PM_{2.5}$	24 h/daily	Jan and Jul 2003	12/52	4.7/13	4.9/11	No	(5)
Wuhan (30.5° N, 114.2° E)	$PM_{2.5}$	24 h/daily	Jan and Jul 2003	5.6/26	4.0/10	5.4/13	No	(5)
Hangzhou (30.2° N, 120.1° E)	$PM_{2.5}$	24 h/daily	Jan, Jul, and Aug 2003	6.5/24	1.7/4.6	3.2/7.6	No	(5)
Shanghai (31.2° N, 121.4° E)	$PM_{2.5}$	24 h/daily	Jan and Jul 2003	5.6/21	1.8/2.9	3.5/6.8	No	(5)
Nanning (22.82° N, 108.35° E)	PM_{10}	24 h/every 3 days	2006	3.7/15	1.5/5.8	2.4/7.0	No	(3)
Guangzhou (23.1° N, 113.2° E)	$PM_{2.5}$	24 h/daily	Jan and Jul 2003	8.9/26	2.4/7.0	4.3/9.2	No	(5)
Panyu (23° N, 113.35° E)	PM_{10}	24 h/every 3 days	2006	8.9/21	2.5/7.3	4.6/11	No	(3)
Hong Kong (22.2° N, 114.1° E)	$PM_{2.5}$	24 h/daily	Jan, Jul, and Aug 2003	4.7/9.3	1.1/3.6	1.8/4.8	No	(5)
Xiamen (24.4° N, 118.1° E)	$PM_{2.5}$	24 h/daily	Jan, Jul, and Aug 2003	3.3/11	1.3/4.3	1.7/4.1	No	(5)

ACPD
11, 28219–28272, 2011

Table 3. Footnotes.

[a] Geographical locations of these observation sites are shown in Fig. 4.

[b] Aerosol size sampled: particulate matter with aerodynamic diameter <10 µm (PM_{10}), particulate matter with aerodynamic diameter <2.5 µm ($PM_{2.5}$), and total suspended particles (TSP).

[c] Observed annual mean concentrations are calculated by averaging available monthly mean observations. For observations by Cao et al. (2007), January and July concentrations are averaged to calculate each annual mean.

[d] Simulated annual mean concentrations are calculated by averaging results from the months used to calculate the observed annual means at each site.

[e] (1) Qu et al. (2008); (2) Cao et al. (2009); (3) Zhang et al. (2008); (4) Y. M. Han et al. (2008); (5) Cao et al. (2007).

[f] At Muztagh Ata each filter sample was nominally collected over a one week period. However, during periods when the solar power supply was insufficient, the samples were regarded as valid and analyzed when the sampling standard air volume was larger than 30 m^3 (Cao et al., 2009).

[g] Measurements were made at Muztagh Ata from Dec 2003 to Feb 2006. Only data from 2005 is used in this study.

[h] Gucheng site is at a rural location but within an area of rapid urbanization according to Zhang et al. (2008). Its EC and OC concentrations are very high and show obvious influence from local sources. We categorize it as an urban site for this study.

ACPD
11, 28219–28272, 2011

Table 4. Estimates of Chinese anthropogenic carbonaceous aerosol emissions after the year 2000.

Study	Method	EC/OC emissions (Tg C yr^{-1})							
		2000	2001	2003	2004	2005	2006	2008	2010
Streets et al. (2003a)	Bottom-up	0.94/2.66[a]							
Cao et al. (2006)	Bottom-up	1.40/3.84[b]							
Ohara et al. (2007)	Bottom-up	1.09/2.56[b]		1.14/2.62[b]					
Nozawa et al. (2007)	Bottom-up	1.60[b]/–							
Lamarque et al. (2010)	Bottom-up	1.30/2.80[c]							
Zhang et al. (2009)	Bottom-up		1.60/2.83[b]				1.81/3.22[d]		
Lei et al. (2011)	Bottom-up	1.18/2.54[b]				1.51/3.19[e]			
Lu et al. (2011)	Bottom-up	1.16/2.41[f]			1.47/3.13[g]			1.68/3.37[h]	1.74/3.44[i]
Kondo et al. (2011)	Top-down							1.92[j]/–	
This work	Top-down						2.94/6.42[k]		

[a] Uncertainties, represented as 95 % confidence intervals (CI), are ± 484 % and ± 495 % for EC and OC, respectively.
[b] Uncertainties not reported in paper.
[c] Chinese anthropogenic EC and OC emissions taken from Bond et al. (2007) with updates from T. Bond (personal communication, 2011). Uncertainties are expected to be larger than a factor of 2.
[d] Uncertainties (represented as 95 % CI) are ±208 % for EC and ±258 % for OC, respectively.
[e] Uncertainties (represented as 95 % CI) are ±187 % and ±229 % for EC and OC, respectively.
[f] Uncertainties (represented as 95 % CI) are 0.62–2.29 Tg C yr^{-1} for EC and 1.22–4.70 Tg C yr^{-1} for OC.
[g] Uncertainties (represented as 95 % CI) are 0.80–2.98 Tg C yr^{-1} for EC and 1.57–6.22 Tg C yr^{-1} for OC.
[h] Uncertainties (represented as 95 % CI) are 0.95–3.17 Tg C yr^{-1} for EC and 1.73–6.57 Tg C yr^{-1} for OC.
[i] Uncertainties (represented as 95 % CI) are 0.97–3.31 Tg C yr^{-1} for EC and 1.73–6.78 Tg C yr^{-1} for OC.
[j] Top-down BC emission estimate based on measurements at Cape Hedo Observatory, Japan from February 2008 to May 2009. The estimated uncertainty is 40 %.
[k] Uncertainties, represented as standard deviations, are ±0.60 Tg yr^{-1} for EC and ±1.10 Tg C yr^{-1} for OC. The corresponding 95 % CI (calculated assuming normal distribution) are ±40 % for EC and ±34 % for OC, respectively. See text for details.

ACPD
11, 28219–28272, 2011

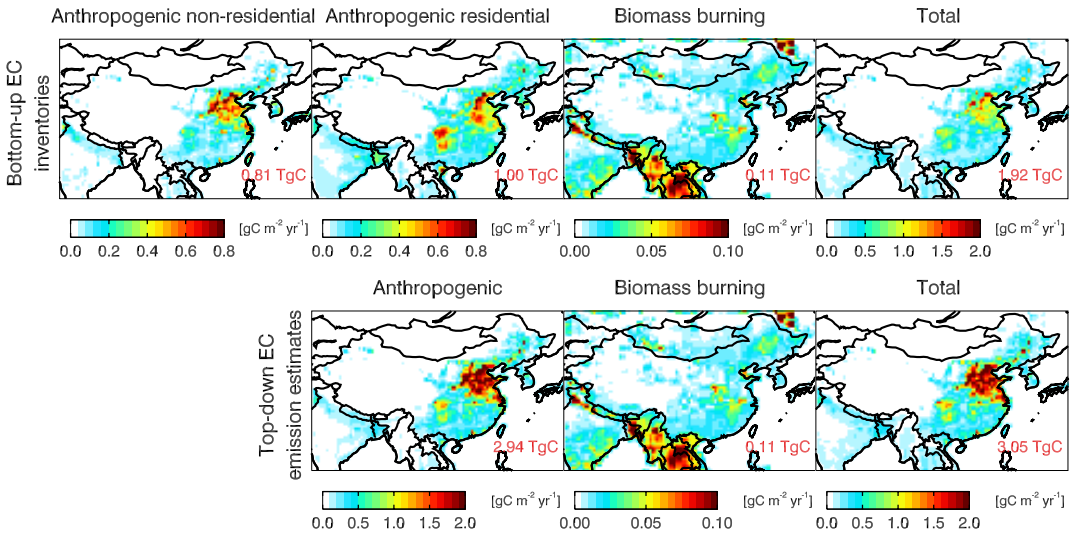

Fig. 1. Annual emissions of EC from China. Top panel: bottom-up inventories of Zhang et al. (2009) (anthropogenic) and Streets et al. (2003b) (biomass burning). Bottom panel: emissions inferred from surface EC obserations on the basis of the multiple regression analysis in this study. Biomass burning emission is unchanged because no observational constrain is available. Chinese annual emission totals are shown inset in red.

ACPD
11, 28219–28272, 2011

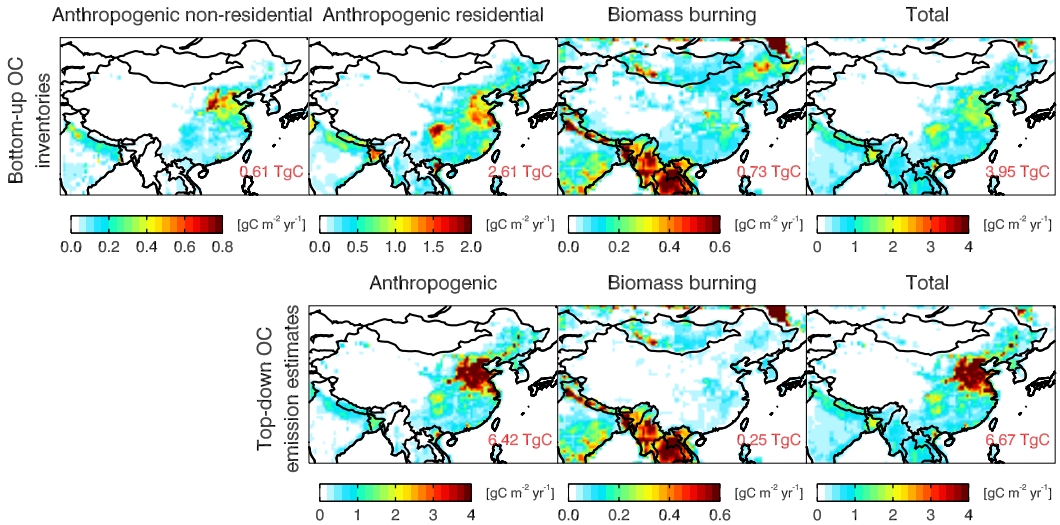

Fig. 2. Annual emissions of OC from China. Top panel: bottom-up inventories of Zhang et al. (2009) (anthropogenic) and Streets et al. (2003b) (biomass burning). Bottom panel: OC emissions inferred by scaling top-down EC emission estimates with observed primary OC/EC ratios by Cao et al. (2007). See text for details. Chinese annual emission totals are shown inset in red.

ACPD
11, 28219–28272, 2011

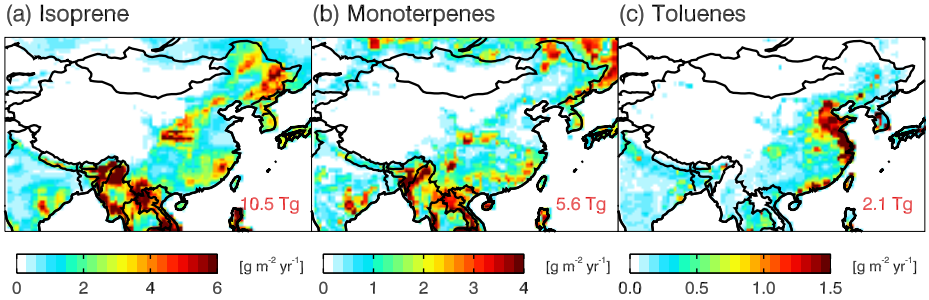

Fig. 3. Annual emissions of **(a)** biogenic isoprene, **(b)** biogenic monoterpene, and **(c)** anthropogenic and biomass burning toluene in the model. Chinese annual emission totals are shown inset in red.

ACPD
11, 28219–28272, 2011

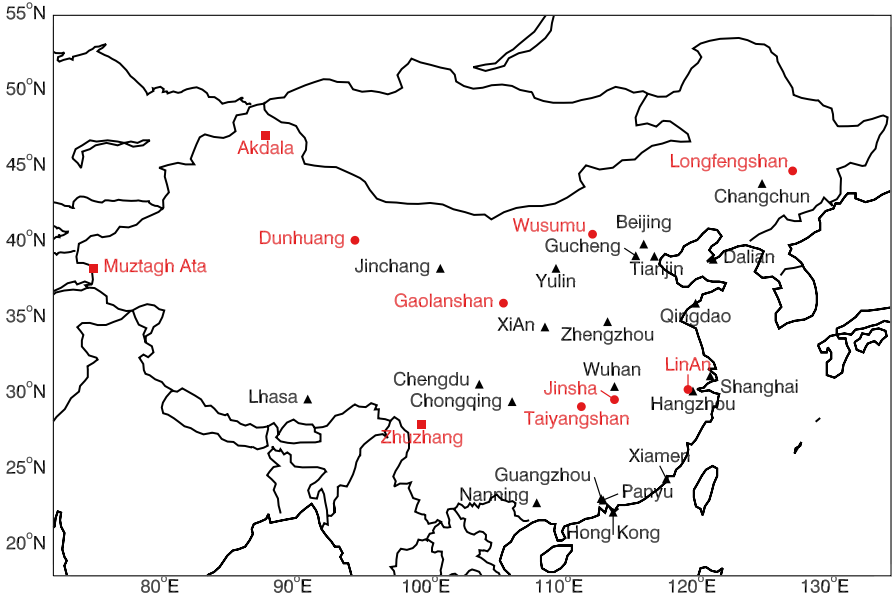

Fig. 4. Locations of the Chinese surface measurement sites used in this study, including three background sites (red squares), seven rural sites (red circles), and twenty-one urban sites (black triangles).

ACPD
11, 28219–28272, 2011

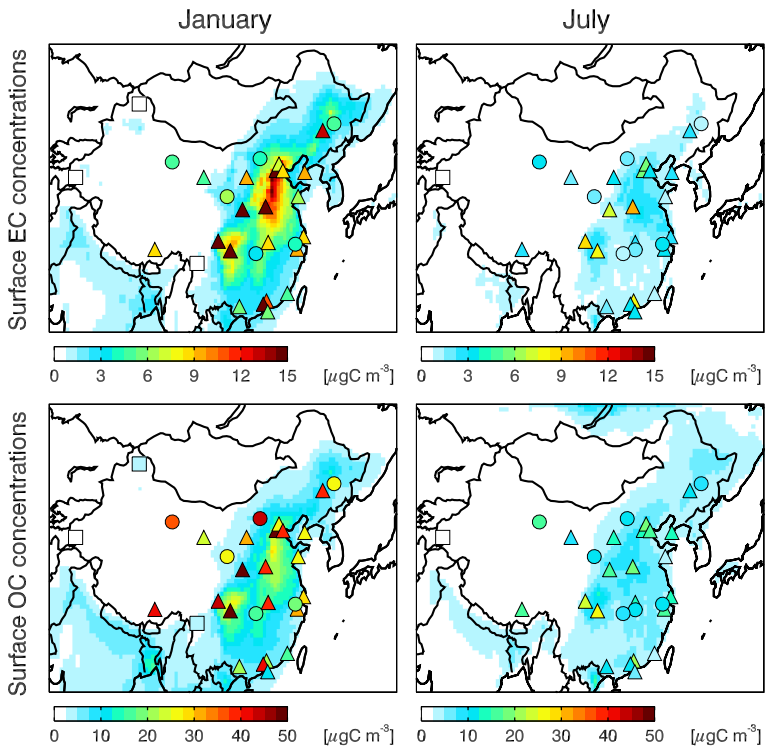

Fig. 5. Observed surface EC (top) and OC (bottom) concentrations in January and July at background (squares), rural (circles), and urban (triangles) Chinese sites. Underlain are simulated EC and OC monthly mean concentrations for January and July 2006 using bottom-up emission inventories.

ACPD
11, 28219–28272, 2011

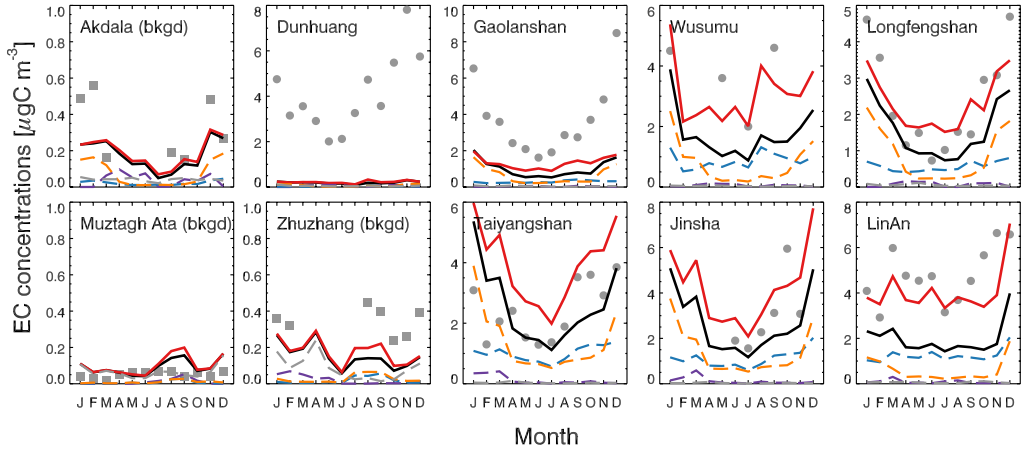

Fig. 6. Monthly mean surface EC concentrations observed at ten Chinese background (grey squares) and rural (grey circles) sites. Solid lines indicate the simulated monthly mean concentrations using bottom-up emission inventories (black) and top-down emission estimates (red). Also shown are simulated components of surface EC concentrations: Chinese anthropogenic residential (orange dashed), Chinese anthropogenic non-residential (blue dashed), Chinese biomass burning (purple dashed), and contributions from non-Chinese sources (gray dashed).

ACPD
11, 28219–28272, 2011

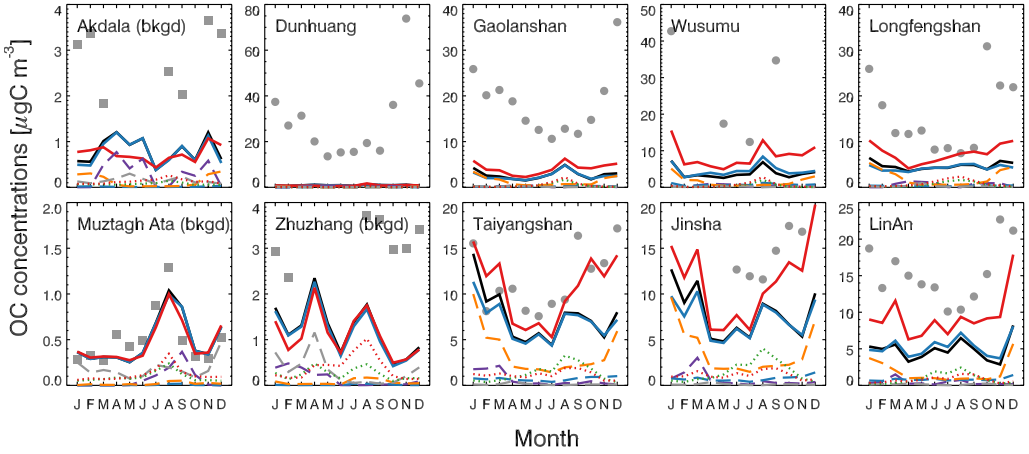

Fig. 7. Monthly mean surface OC concentrations at ten Chinese background (grey squares) and rural (grey circles) sites. Solid lines indicate simulated monthly mean concentrations using bottom-up emission inventories (black), top-down emission estimates (red), and hybrid emission estimates (blue). Also shown are simulated components of surface OC concentrations: Chinese anthropogenic residential (orange dashed), Chinese anthropogenic non-residential (blue dashed), Chinese biomass burning (purple dashed); semi-volatile SOC (green dotted), dicarbonyl SOC (red dotted), and contributions from non-Chinese sources (gray dashed).

ACPD
11, 28219–28272, 2011

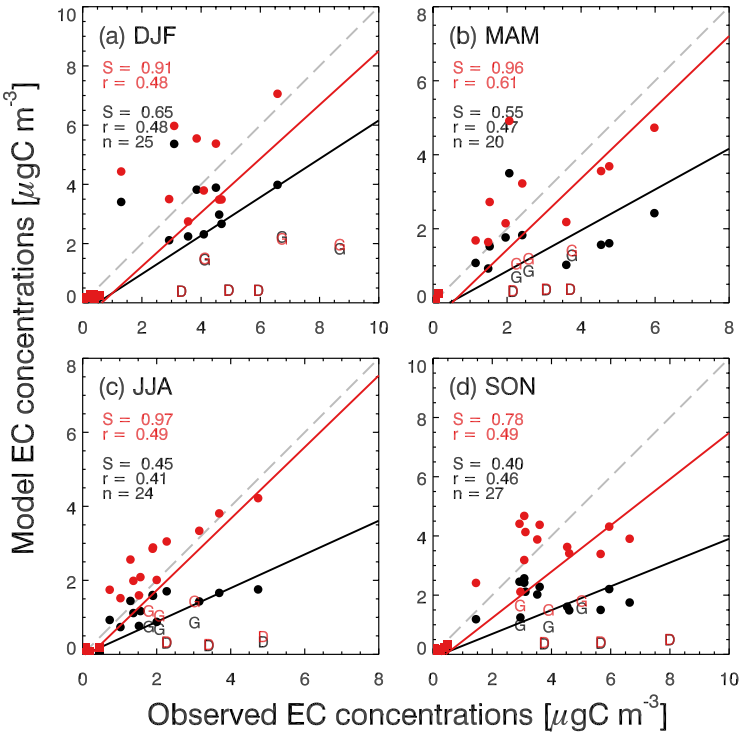

Fig. 8. Simulated versus observed monthly mean surface EC concentrations at rural (circles; Gaolanshan: G; Dunhuang: D) and background (squares) sites and the reduced-major axis regression lines (solid lines) for each season. Black: model results using bottom-up emission inventories; red: model results using top-down emission estimates. The reduced major-axis regression slope (S) and correlation coefficient (r) between model and observation, and number of data points (n) for each season are shown inset. Grey dashed line indicate the 1:1 line.

ACPD
11, 28219–28272, 2011

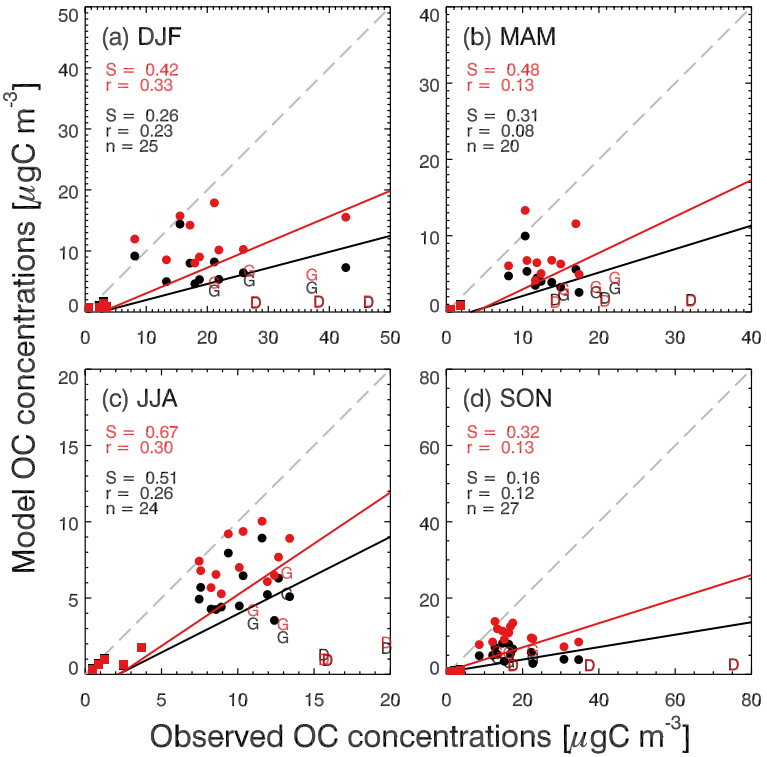

Fig. 9. Scatterplots of simulated versus observed monthly mean surface OC concentrations at rural (circles; Gaolanshan: G; Dunhuang: D) and background (squares) sites and the reduced-major axis regression lines (solid lines) for each season. Black: model results using bottom-up emission inventories; red: model results using top-down emission estimates. The reduced major-axis regression slope (S) and correlation coefficient (r) between model and observation, and number of data points (n) for each season are shown inset. Grey dashed line indicate the 1:1 line.

ACPD
11, 28219–28272, 2011

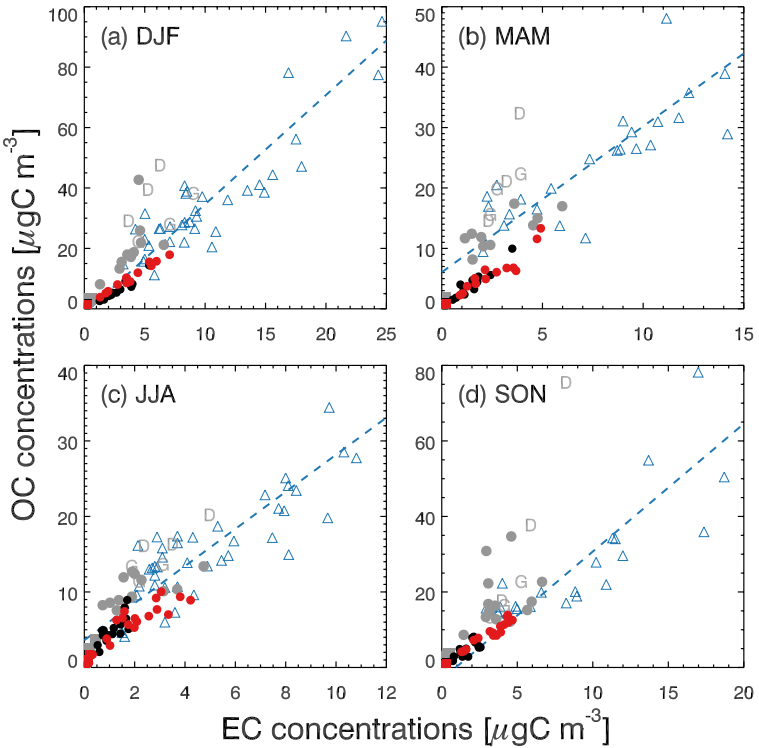

Fig. 10. OC versus EC concentrations observed (grey circles; G: Gaolanshan; D: Dunhuang) and simulated using bottom-up (black) and top-down (red) emissions at rural and background sites for each season. Also shown are observed OC versus EC concentrations (blue triangles) and reduced major-axis regression lines at urban sites (blue dashed lines) for each season.

ACPD
11, 28219–28272, 2011

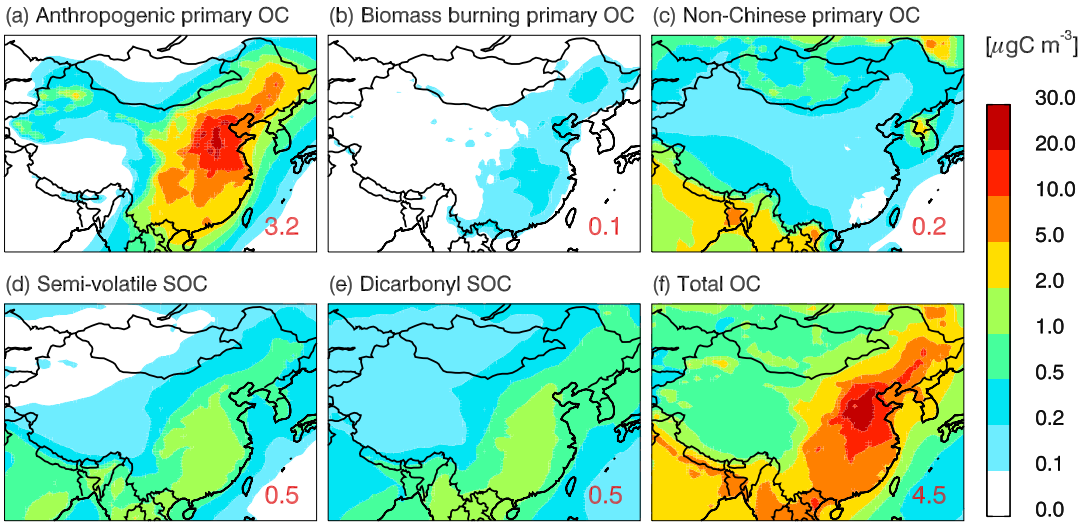

Fig. 11. Simulated components of surface annual mean OC using top-down emission estimates: **(a)** Chinese anthropogenic primary OC (including residential and non-residential sources); **(b)** Chinese biomass burning primary OC; **(c)** non-Chinese primary OC; **(d)** semi-volatile SOC from biogenic and anthropogenic VOC precursors; **(e)** SOC from irreversible uptake of dicarbonyls by aqueous-phase particles (mainly in clouds); and **(f)** total simulated OC. Simulated Chinese annual mean surface concentrations for each component are shown inset in red.

ACPD
11, 28219–28272, 2011